heliotek

CR 114475
Available to the Public

Research and Development of Silicon Solar Cells for Low Solar Intensity and Low Temperature Applications

by P. Payne

February, 1972

Final Report

Distribution of this report is provided in the interest of information exchange. Responsibility for the contents resides in the author or organization that prepared it.

Prepared under Contract No. NAS2-5519

by

Heliotek, Division of Textron, Inc.
12500 Gladstone Avenue
Sylmar, California 91342

for

AMES RESEARCH CENTER
NATIONAL AERONAUTICS AND SPACE ADMINISTRATION

(NASA-CR-114475) RESEARCH AND DEVELOPMENT OF SILICON SOLAR CELLS FOR LOW SOLAR INTENSITY AND LOW TEMPERATURE APPLICATIONS Final Report P. Payne (Heliotek) Feb. 1972 77 p CSCL 10A G3/03
N72-27065
Unclas
34301

SUMMARY

The work performed during this contract included identifying the problems encountered in using N/P solar cells at low temperature and low intensity, solving these problems, and incorporating the solutions in a manufacturing procedure.

Theoretical analysis of the effects of low temperature and low intensity on the various solar cell characteristics indicated that the following behavior might be expected: 1) lower short circuit current, 2) higher open circuit voltage, 3) series resistance becoming less significant, and 4) shunt resistance becoming more critical.

From the theoretical analysis, variations in shunt resistance was the only factor expected to produce significant variations in output; however, in the initial work, three other problem areas were quickly identified: 1) formation of a metal-semiconductor barrier, 2) variations in short circuit current at -135°C, and 3) excess current flow at -135°C starting between .2 and .4 V ("broken knee" effect).

High resistance or rectifying contacts due to metal-semiconductor barrier formation was a problem encountered at low temperature with standard TiAg contacts. Ohmic contact can be obtained if the dopant concentration at the surface is very high, so Al was alloyed into the silicon to form a P+ region. This improved the V_{oc} by ~100 mV at 5 mW/cm^2 and -135°C and increased the maximum power voltage from ~ .7 V to .8 V. The procedure of alloying Al into the silicon to form an ohmic contact was simple and processing parameters did not seem extremely critical; with Al film thicknesses of of ~.1μ and above, alloy temperatures as low as 600°C could be used. Ohmic contact could also be achieved by evaporating the Al and TiAg in one evaporation run and then merely sintering the contact at ~ 600°C.

Low shunt resistance due to current leakage paths across the junction is more critical at low intensity because the leakage current can be a significant portion of the light generated current. During this contract two methods for reducing leakage current were investigated: 1) increasing the junction depth, and 2) etching the cell edges to remove any metal contamination. By increasing the junction depth from ~ 0.5 to 1.0 μM, the average leakage current of 2 x 2 cm cells measured at .7 V in the dark was reduced from ~ 50 to 10 μA. An edge etching technique was then developed which was effective in reducing the leakage current due to metal on the cell edges as well as the low temperature excess current flow starting between .2 and .4 V, referred to as the double slope, or broken knee effect.

The wide range in I_{sc} observed at -135°C was due to variations in $\Delta I_{sc} / \Delta T$. Comparison of cricible grown to Mon-X and float zone cells showed much less variation of $\Delta I_{sc} / \Delta T$ for the Mon-X and float zone cells. Crucible grown cells with currents (at 5.0 mW/cm^2 intensity) of ~ 4.3 mA at 28°C exhibited currents of 2.0 to 3.9 mA at -135°C; float zone and Mon-X cells also with short circuit currents of ~4.3 mA had currents of 3.6 to 3.9 mA at -135°C.

In the pilot production phase five lots of 100 cells were fabricated. The following process additions or modifications were made to obtain improved low temperature and low intensity performance: 1) silicon slabs were etched prior to slicing in order to reduce damage at cell edges; 2) a 2-hour rather than 32-minute diffusion was used to reduce leakage current; 3) Al was included in the TiAg contact system in order to obtain contacts which were ohmic at low temperature; 4) after contact evaporation cells were edge etched in order to reduce not only leakage currents due to metal across the junction at the cell edge cells but, also, the "broken knee" effect which was characterized by excess current flow at .2 to .4V. Prior to edge etching the majority of cells in all five lots exhibited excessive dark current at -196°C, .5 mA or greater at .9 V, correlating to low output at 5.0 mW/cm^2 and -135°C. Once edge etched ~ 70% of the cells had outputs of 2.8 mW or better; this corresponds to a cell efficiency (based on total cell area of 4 cm^2) of 14%. This pilot production phase demonstrated that cells with improved performance at low temperature and low intensity can be fabricated on a production basis.

Once fabrication of the cells was completed, samples from each lot were subjected to typical qualification tests to determine whether any of the process modifications had changed the cell behavior. Tests performed included 45° pull, temperature cycling from -140 to +85°C, and 30 day humidity exposure at 45°C, 90% relative humidity. In all these tests the average cell degradation was less than 1%.

TABLE OF CONTENTS

List of Illustrations

List of Tables

1.0 INTRODUCTION

With present manufacturing methods solar cells are produced with typical AMO efficiencies of 9 to 10% at 60°C (typical operating temperature in space). Spacecraft missions to Jupiter present totally different operating conditions, -135°C rather than 60°C, and 5.0 mW/cm^2 instead of 140 mW/cm^2 solar intensity. Since these drastic changes in operating conditions would have varying impact upon the different solar cell characteristics such as series and shunt resistance, a re-evaluation of cell behavior was needed. Some of the effects could be theoretically predicted. For example, according to theory, series resistance becomes less significant and shunt resistance more significant with decreasing light level and these opposite trends indicate a possible trade-off in terms of junction depth. With series resistance becoming less significant, a shallower junction could be used to obtain higher short circuit current; on the other hand, with very shallow junctions the shunt resistance is typically lower, and this would lead to a lower fill factor and lower output.

However, identification of the problems or in some cases, merely the effects, had to be a combination of theory and experimental observation. For example, theory predicts a decrease in Isc with temperature, but gives no indication of the observed wide range in I_{sc} at -135°C due to variations in the thermal coefficient of short circuit current.

The problems which were understood in terms of cause and effect were investigated and solved first. Then models were established and tested for those problems which were only identified in terms of effects.

The contract objectives included not only identifying and solving the problems producing low cell output at low temperature and low intensity, but also incorporation of these solutions into a new manufacturing process. The new manufacturing process was then tested in a pilot production phase, which also provided statistical data on cell performance.

2.0 TECHNICAL DISCUSSION

2.1 BACKGROUND

The purpose of this program was to obtain a solar cell design optimized for operation at 5.0 mW/cm^2 solar intensity and -135°C temperature, corresponding to the Jupiter environment. Generally, solar cells had been built for near earth or 1 AU environments and little consideration had been given to the problems likely to be encountered by cells operating at very low temperatures and low solar intensities.

From work performed previous to this program[1-4], there were strong indications that wide variations in performance of silicon solar cells could be expected at low levels of temperature and illumination. It was observed that conventional cells with similar AMO conversion efficiencies could vary over an order of magnitude in conversion efficiency (1 to 15%) under Jupiter conditions (5 mW/cm^2, -135°C).

To determine what might be expected at low temperature and illumination, each component of the solar cell equivalent circuit (Fig. 1) was examined. Basically there are four elements that play important roles in determining the behavior of a typical solar cell and each was examined.

2.1.1 Current Generator

The solar cell is a direct solar energy converter and the amount of current generated is proportional to the intensity of the useful incident radiation. Thus the influence of low illumination levels on the cell current is a simple linear relationship. The dependence of current (I_{sc}) on temperature is much more complicated. Since I_{sc}

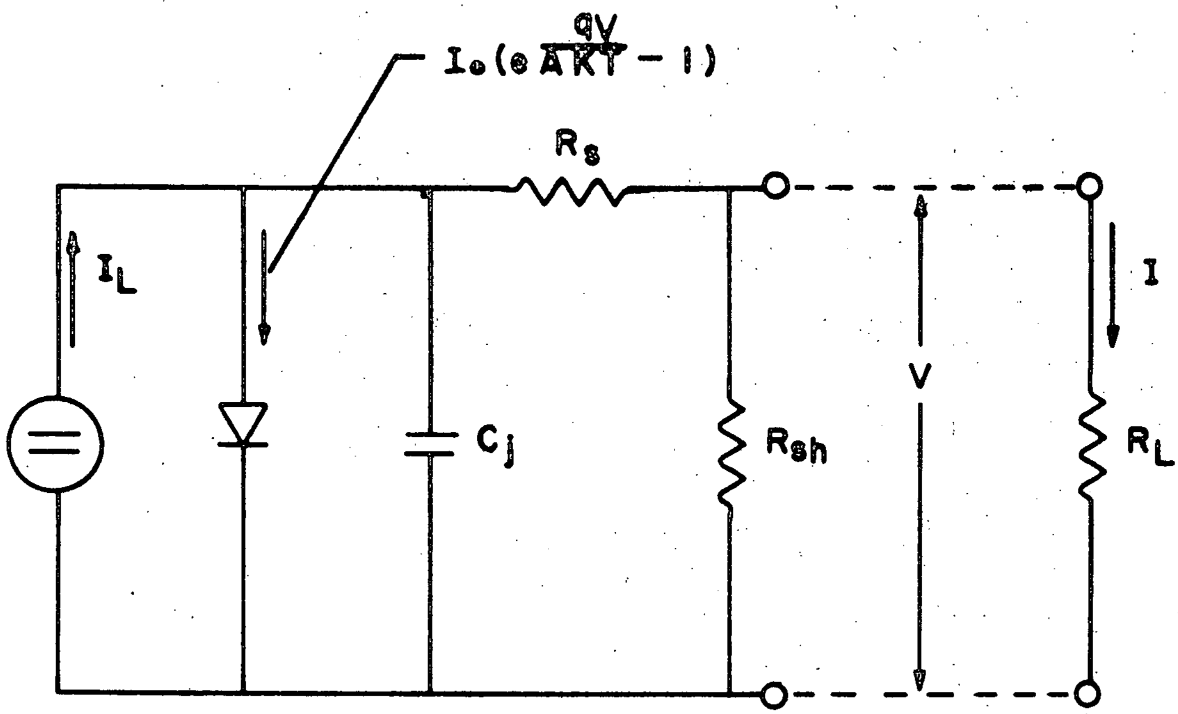

SOLAR CELL EQUIVALENT CIRCUIT

$$I = I_o\left(e^{\frac{q(V - IR_s)}{AKT}} - 1\right) + \frac{V}{R_{sh}} - I_L$$

DESCRIPTIVE EQUATION

FIGURE 1

is directly related to minority carrier lifetime, we can use expressions for lifetime such as:

$$\text{n-region} \quad \tau = \tau_{po} \left[(1 + \exp (E_T - E_F/kt) \right]$$

$$\text{p-region} \quad \tau = \tau_{no} + \tau_{po} \exp (E_T + E_F - 2E_1/kt)$$

where E_T = trap level

E_F = Fermi energy

E_i = intrinsic energy level

τ_{po} = hole lifetime in material in which all traps are full

τ_{no} = electron lifetime in material in which all traps are empty

to relate the behavior of current at very low temperatures. It can be seen that expressions such as this are complicated functions of temperature and at best can predict general trends only.

2.1.2 Diode Element

The diode component of the solar cell equivalent circuit plays a critical role in determining the open circuit voltage (V_{oc}) of the cell. It has been shown that the following expression describes V_{oc} fairly reliably:

$$V_{oc} = \frac{AKT}{q} \ln (I_L/I_o + 1)$$

where I_L is the generated current, and I_o is the reverse saturation current of the diode. Since I_o is a very strong funtion of temperature:

$$I_o \propto T^3 \exp (eEo/kT)$$

we would expect that V_{oc} would increase as the temperature was reduced.

Even though I_L, the generated current, is related logarithmically to the voltage, and the voltage will decrease logarithmically with illumination level, the net effect will still be an increase in open circuit voltage.

2.1.3 Shunt Resistance

This element represents a leakage path for the generated current, I_L. At high light levels the leakage current is in most cases a small fraction of the light generated current. However, at low illumination levels the leakage current can become a significant portion of the total generated current and influence the I-V curve shape of the solar cell. As will be shown in a later section of this report, variations in shunt resistance play a key role in the cell efficiency at Jupiter conditions.

2.1.4 Series Resistance

At high light levels series resistance is the dominant factor influencing the curve shape of the cell. It manifests itself as a voltage drop (IR_s) and thus for conditions where there is a large light generated current it is extremely important. However, at low light levels, the linear reduction in generated current makes series resistance less effective since now the cell voltage is still a large fraction of its initial high light level value. Coupling this with the fact that low temperatures further increase open circuit voltage, the effect of series resistance is minimized further.

2.1.5 Summary

One can conclude from theory that a standard solar cell would exhibit the following behavior upon operation at Jupiter conditions (-135°C) 5mW/cm^2). The short circuit current would decrease at a greater than linear rate due to the influence of low temperature. The open circuit voltage would increase due to the reduction in reverse saturation current, although the total improvement in voltage would be modified by the logarithmic decrease in voltage caused by the lowered illumination level. The I-V characteristic would improve if the cell were dominated by series rather than shunt resistance, at AMO and room temperature. Cells with high leakage currents at room temperature would show relatively poor curve shapes at Jupiter conditions. From the preliminary conclusions to which our brief analysis leads, the reported large variation in cell efficiencies at low temperatures and light levels can be understood.

2.2 EXPERIMENTAL OBSERVATIONS

Initial work on conventional solar cells quickly identified four major problem areas at Jupiter test conditions. In brief they were:

1. The formation of a metal-semiconductor barrier at low temperatures which reduced both the maximum power voltage (V_{mp}) and the open circuit voltage, (V_{oc}).
2. Severe variations in shunt resistance which for cases of low shunt resistance resulted in lower than expected open circuit voltages as well as a reduction in the fill factor of the I-V curve.
3. Cell to cell variations in the short circuit current (I_{sc}) temperature coefficient which yielded a wide range in I_{sc} values for both Jupiter (5 mW/cm^2) and normal (140 mW/cm^2) intensities.
4. A "broken knee" effect which reduced both the current and voltage at maximum power. It was characterized by excess current flow starting between 0.2 and 0.4 volts.

2.2.1 Metal-Semiconductor Barrier Formation

One characteristic of plated and evaporated contacts is that while they may be ohmic at room temperature, they can develop high resistance or become rectifying at low temperatures.[5]

This is due to the formation of a barrier at the metal-semiconductor interface. The effect on solar cell performance is reduction of both open circuit voltage and voltage at maximum power at low temperatures.

This barrier is present to a large degree at room temperature with all cells after the TiAg metal contact deposition but it is essentially eliminated by a sintering procedure. At low temperature the barrier reappears in varying degrees and is exaggerated by the relatively high resistance of the silicon base region (10 ohm cm).

2.2.1.1 Methods for Eliminating Metal-Semiconductor Barrier

Ohmic contact can be made if the impurity concentration at the semiconductor surface is very large.[6] In P-type silicon this can be accomplished by diffusing a dopant, such as boron, or alloying Al into the back surface. Evaporation and alloying Al to form the P+ region was investigated since fewer and simpler processing steps and lower processing temperatures would be required than for a boron diffused P+ region.

Cells were fabricated in the following manner: $\sim .1 \mu M$ of Al was evaporated, and then alloyed at $\sim 600°C$; the excess Al was removed and then TiAg contacts were applied. I-V curves were measured at both high and low intensity and the forward characteristic exhibted no sign of high resistance or rectification. As shown in Figure 2, the open circuit voltage was linear with temperature.

2.2.1.2 Al Alloying: Film Thickness and Temperature

Once the metal-semiconductor barrier was eliminated, experiments were performed to define the limits of the alloying process. The two most important parameters were the thickness of the alloy region and the alloying temperature. The first parameter is a

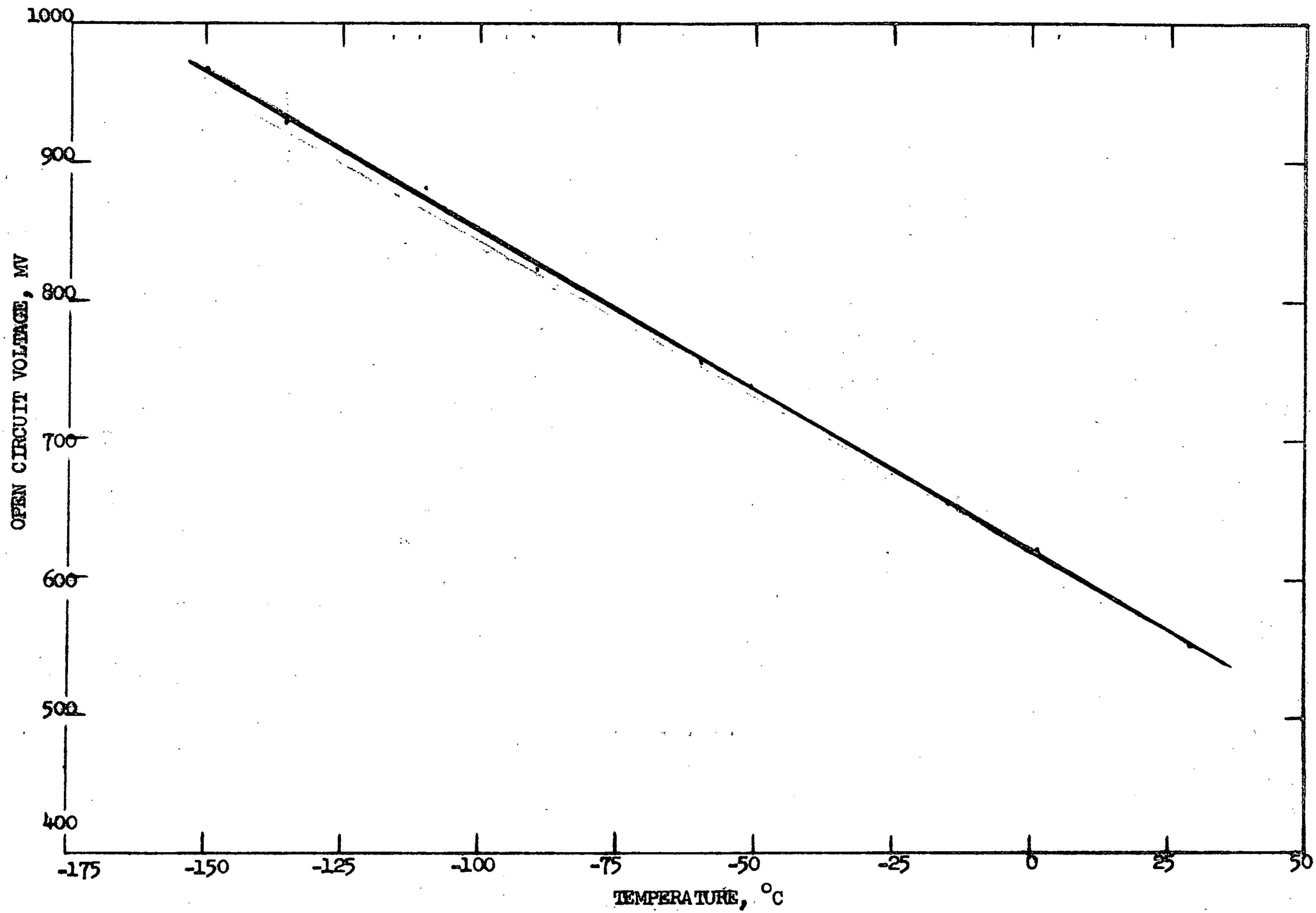

Figure 2 V_{oc} vs. Temperature for P^+ Cells.

strong function of the amount of material available to alloy with the silicon as well as the alloying temperature used. The second parameter had great practical importance since if the alloy temperature could be made comparable to the typical sintering temperature of TiAg the new process could be installed with a minimum impact on production processes. Al layer thicknesses of ~.01, .06, .10, .25 and 1.0 μM were deposited upon the diffused blanks and then heated at ~600°C for 5 minutes. After heating, TiAg contacts were applied and I-V curves were obtained between +28 and -135°C at both high and low intensity. Al film thicknesses of .01 and .06 μM did did not produce ohmic contact at low temperatures; but film thickness of .1 to 1.0 μM did.

Samples with various Al film thicknesses were also heated to ~600°, 650° and 700°C for 5 minutes. The results are summarized in Table 1. A temperature of 700°C produced extremely high leakage currents resulting in low open circuit voltage, curve factor, and output. The open circuit voltage of cells with the Al heated to ~650°C was linear with temperature, and unlike the cells with the Al heated at 600°C, good low temperature ohmic contacts were achieved with the .01 and .06 μM thick Al films.

2.2.1.3 Production Considerations

In terms of a production process, application of the contact materials, including the Al, in one evaporation (one-step) would be preferable to separate evaporation and alloying of the Al prior to deposition of the TiAg contacts (two-step). A single evaporation step could be used if in the normal TiAg sintering operation the Al alloyed into the silicon and formed a contact which was ohmic at low temperatures. The two procedures were compared.

The sintering or alloying temperature was 600°C, which is typically used for TiAg contacts, and the thickness of the evaporated Al film was ~0.1 μM since thinner films when heated to only 600°C did not

TABLE I

Experiment #20 - Thickness of Aluminum Layer vs. Alloy Temperature

Variable 650° - Alloy Temp.	Cell #	I_R (dark)[4] μA +28°C	I_R (dark)[4] μA -135°C	I_{sc} mA +28°C	I_{sc} mA -135°C	V_{oc} mV -135°C	Maximum Power-mW -135°C	Curve Factor +28°C	Curve Factor -135°C	Remarks B[1]	Remarks D.S.[2]	Remarks R.K.[3]
.01μ Aℓ	1	37	11	4.3	3.0	845	1.93	0.719	0.751	-	x	-
.06μ Aℓ	5	21	4	4.4	2.8	855	2.03	0.776	0.799	-	-	-
.12μ Aℓ	9	12	4	4.3	2.4	835	1.65	0.746	0.825	-	-	-
.12μ Aℓ	22	19	6	4.3	2.7	858	1.97	0.747	0.851	-	-	-
.12μ Aℓ	23	10	5	4.3	2.2	840	1.42	0.734	0.772	-	-	x
.12μ Aℓ	24	270	320	4.6	3.2	863	1.92	0.717	0.697	-	-	x
.12μ Aℓ	25	19	8	4.2	2.6	840	1.55	0.714	0.714	-	x	x
.12μ Aℓ	26	455	730	4.3	2.6	835	1.15	0.664	0.531	-	-	-
.12μ Aℓ	27	140	80	4.4	2.5	853	1.55	0.708	0.607	-	x	x
.25μ Aℓ	13	39	25	4.5	3.0	852	2.11	0.765	0.825	-	-	-
1.0μ Aℓ	17	27	7	4.3	2.6	790	1.53	0.709	0.746	-	-	x
Variable 700° - Alloy Temp.												
.06μ Aℓ	7	350	370	4.3	3.0	815	1.50	0.723	0.644	-	-	x
.12μ Aℓ	11	740	1200	4.4	2.7	795	.82	0.667	0.381	-	-	x
.12μ Aℓ	30	960	1310	4.3	2.7	819	.98	0.666	0.447	-	-	-
.12μ Aℓ	33	1750	2430	4.5	2.6	742	1.16	0.594	0.601	-	-	-
.12μ Aℓ	34	900	940	4.6	2.9	830	1.14	0.654	0.473	-	-	-
.25μ Aℓ	15	1050	1500	4.5	2.8	768	.80	0.613	0.372	-	-	x
1.0μ Aℓ	20	720	800	4.4	2.6	535	.68	0.581	0.494	-	-	x

1 B: Barrier
2 D.S.: Double Slope
3 R.K.: Rounded Knee
4 Dark reverse current measured at .7V.

Intensity: 3.85 mW/cm^2
Tungsten Light Source

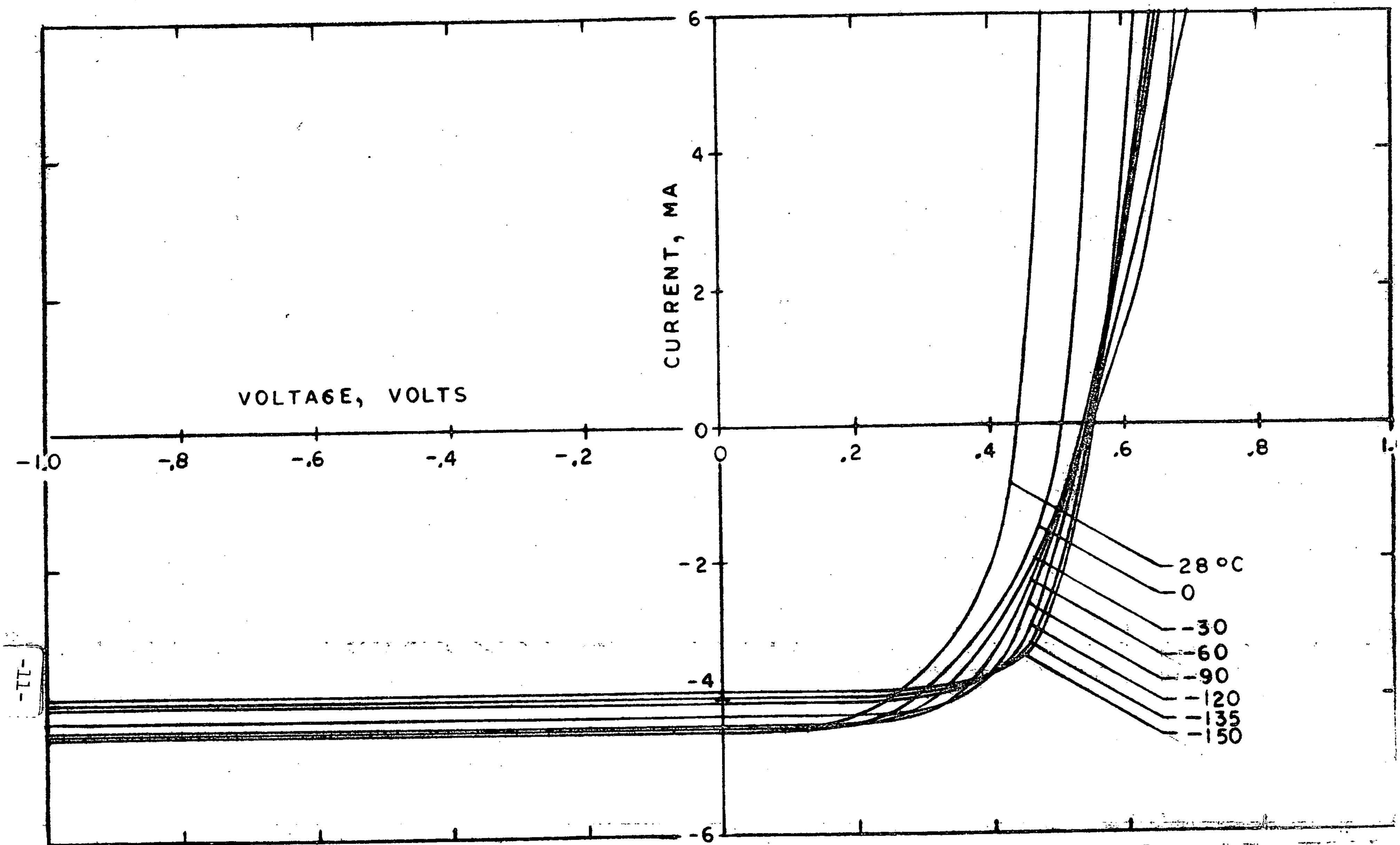

Figure 3. I-V Characteristic Curves at 5.0 mW/cm^2 of P+ Cell with Extreme Broken Knee

produce ohmic contact at low temperature. With both procedures the best cell outputs were in the same range; however, there were more reject cells using the two-step evaporation procedure, due to poor electrical characteristics at low temperature and low intensity as shown in Figure 3. The one-step procedure was selected as the better process since it resulted in good efficiencies and a lower reject rate and also was the more desirable process with respect to production.

2.2.1.4 Conclusions

The metal-semiconductor barrier observed at low temperature with TiAg contacted solar cells was eliminated by alloying Al into the back surface. Film thicknesses of 0.1 μM or greater when heated to 600°C, or .01 μM or greater when heated to 650°C produce ohmic contacts. The Al can be evaporated by itself followed by an alloying step or can be included in the TiAg contact evaporation, in which case ohmic contact is achieved in the 600°C sintering step. Open circuit voltages as high as 860 mV at -135°C were achieved using either of these processes.

2.2.2 <u>Junction Leakage Current Effects</u>

Shunt resistance is usually high enough to be of no concern for standard solar cells operated at sunlight intensities of 140 mW/cm^2 and 28°C; however, at low intensity this parameter is highly critical and the acceptable level of performance must be changed. As seen in Figure 4, leakage currents up to 1 mA at .7V can be present at high intensities with no appreciable effects upon the I-V characteristic curve of 2 x 2 cm cells.

2.2.2.1 Experimental Verification of the Effect of Shunt Resistance at Low Intensity

The importance of shunt resistance on V_{oc} at various light levels is shown in Figure 5. The open circuit voltage versus the log of

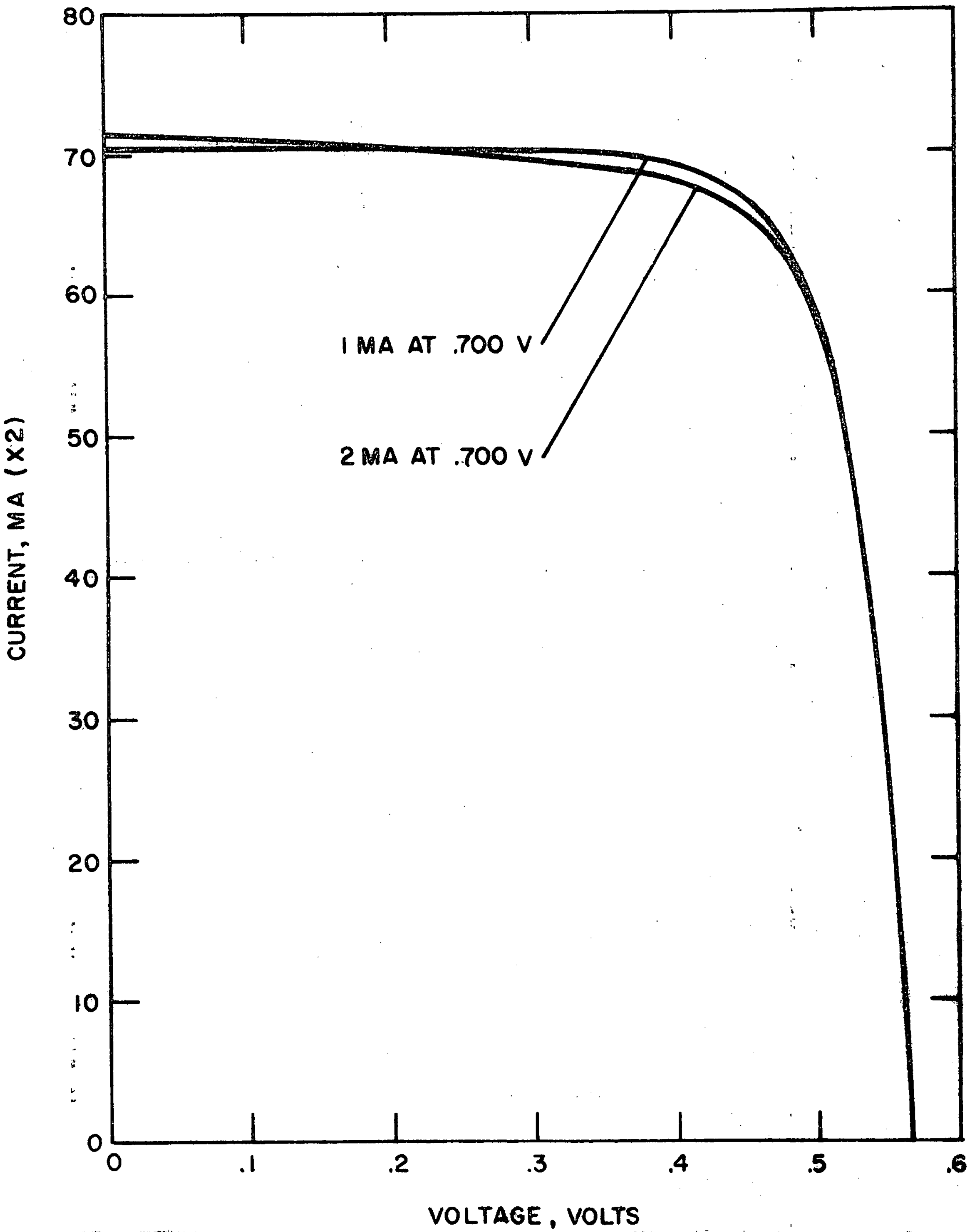

Figure 4. Comparison of cells with two different leakage currents. 10 ohm cm N/P cells (2 x 2 cm) measured in solar simulator at 140 mW/cm^2 and 28°C. C.

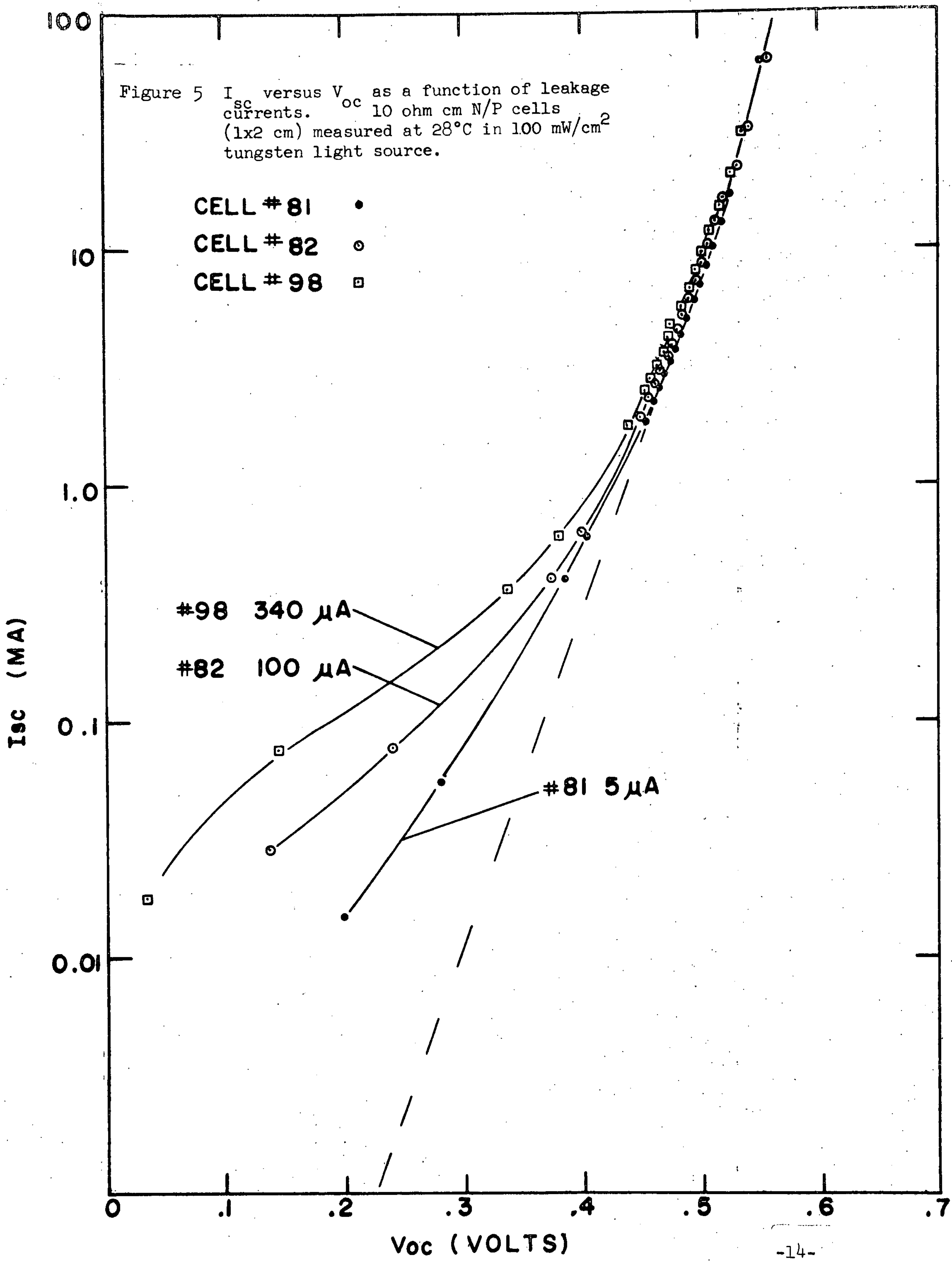

Figure 5 I_{sc} versus V_{oc} as a function of leakage currents. 10 ohm cm N/P cells (1x2 cm) measured at 28°C in 100 mW/cm^2 tungsten light source.

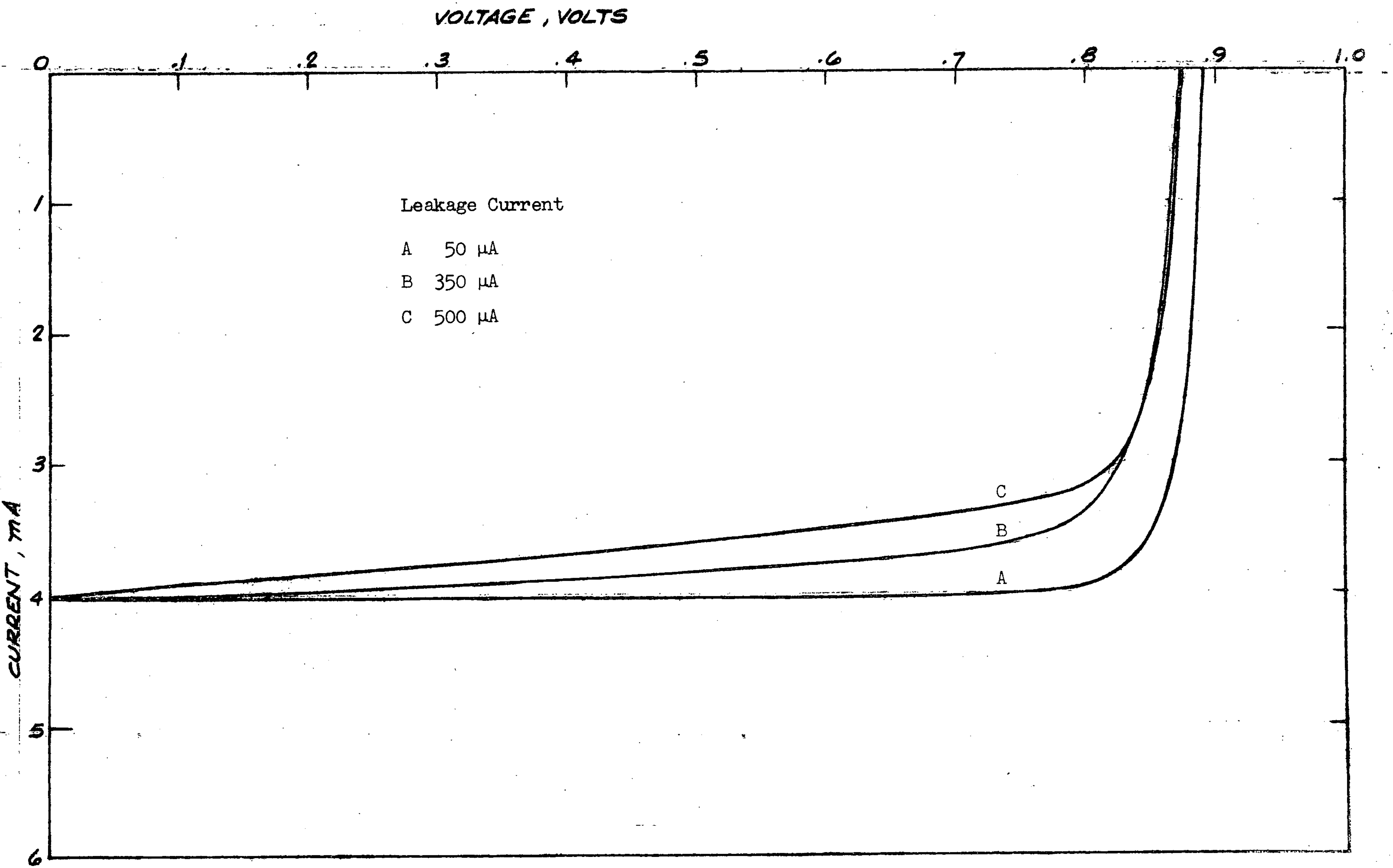

Figure 6. Effect of leakage current (measured at .7V) on I-V characteristic curves of 2 x 2 cm cells. Tested in solar simulator at 5.0m$^{W}/cm^{2}$ intensity and -135°C.

short circuit current relationship is shown for typical 140 mW/cm^2 (one sun) optimized 1 x 2 cm N/P solar cells with leakage currents of 5, 100, and 340 μA at .7V. It can be seen that the V_{oc} decreases much more rapidly with a decrease in light level for the cells with higher dark reverse currents (i.e., lower shunt resistances). From the diode equations one would expect a linear relationship if there was no shunt effect. This linear relationship is approached at higher light levels, but there is significant deviation at lower light levels. The influence of leakage current upon the low intensity, low temperature output is shown in Figure 6. The dark reverse currents of 2 x 2 cm cells measured at .7V at -135°C varied from 25 to 500 μA. Although the short circuit currents measured at 5.0 mW/cm^2 light intensity (X-25)*were within .1 mA of one another (all ~4.0 mA) the difference in current at maximum power (~.8V) was .7 mA. This difference in current at maximum power due to leakage current corresponded to 12.7% efficiency for the cell with 25 μA dark reverse current.

The following are some of the factors which can lead to higher leakage currents; metal across the junction at the cell edges or at a surface scratch, mechanical surface damage which is not completely removed prior to diffusion, improper edge etching, and diffusion of metal atoms or other impurities into the junction region, either during the diffusion or sintering processes.

2.2.2.2 Evaluation of Typical Cells

In order to get an idea of the dark reverse currents obtained on typical high intensity AMO (140 mW/cm^2) type cells, approximately

*Solar Simulator, Spectrolab Model X-25, set to AMO sunlight intensity of 140 mW/cm^2, using a balloon flight calibrated solar cell, and then neutrally filtered to 5.0 mW/cm^2 intensity.

100 N/P 10 ohm cm cells were measured. Sixty of the cells were taken from a group of cells that had an AMO output (X-25, 140 mW/cm^2) of 134-136 mA at 430 mV and 40 cells were taken from a group of cells that had an output of 124-126 mA at 430 mV. Figure 7 shows the dark current at .7V distribution, for these two groups of cells. In the high output group 70% of the cells had at 0.7V, dark reverse currents of 10μA or less, 96% had 40 μA or less. The lower output group had higher dark reverse currents; only 28% were $\leq$ 10 μA and only 55.5% were $\leq$50 μA. Low temperature and low intensity measurements have shown that the Jupiter experimental cells being developed should have dark reverse currents at least as low as the best conventional cells.

2.2.2.3 Junction Depth vs. Leakage Current

Since lower leakage currents are typically achieved with deeper junctions, leakage current as a function of junction depth was investigated. Cells were fabricated with junction depths of ~.25, .50, 1.0 and 2.0μM (~.50μM is typical of current cells optimized for 140 mW/cm^2 AMO intensity). The leakage current behaved as expected with cells having a 2.0μ deep junction exhibiting the lowest leakage current (Figure 8). However, selection of the optimum junction depth cannot be based upon leakage current alone, since short circuit current and output are also influenced by junction depth (see Section 2.4 for more detailed discussion of short circuit current vs. junction depth). Considering both cell output and leakage current, ~1.0μ was selected as the optimum junction depth.

2.2.2.4 **Conclusions**

Leakage currents of 500 μA do not significantly affect the output of cells operating at 140 mW/cm^2; however at 5.0 mW/cm^2 and -135°C, leakage currents of this magnitude can lower cell output 15 to 20%.

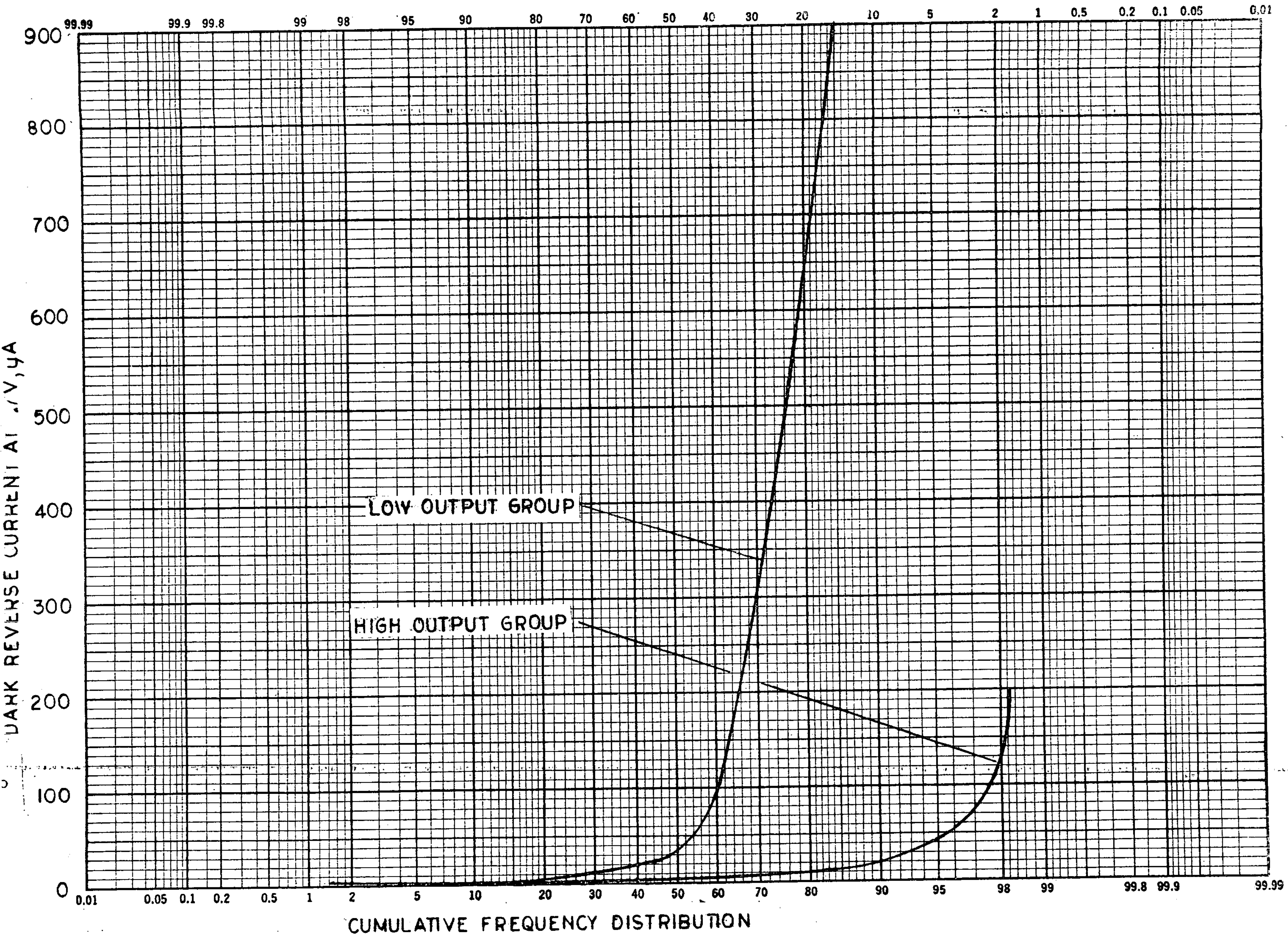

Figure 7 . Distribution of Dark Reverse Currents for Typical AMO (140 mW/cm^2) 2x2 cm Cells. Low output group--40 cells; high output group--60 cells.

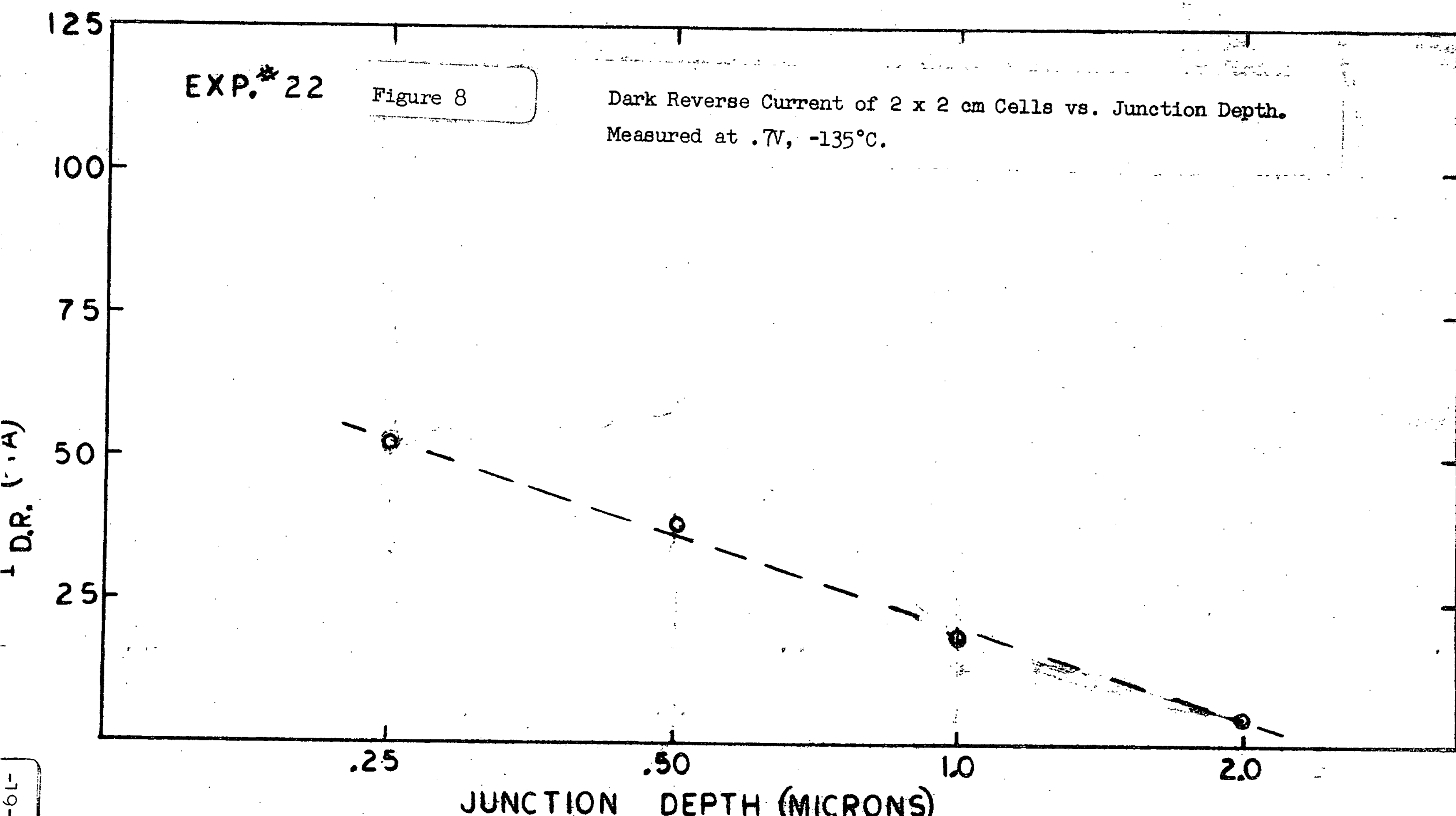

Figure 8

Dark Reverse Current of 2 x 2 cm Cells vs. Junction Depth.
Measured at .7V, -135°C.

Increasing the junction depth by a factor of two from 0.5 to 1.0 μM reduced typical leakage current values from 50 to 25 μA. Cells with deeper junctions which still exhibit high leakage currents typically have metal across the junction at the cell edges. In this case, etching the cell edges to remove the metal contaminants improves cell output.

2.2.3 Broken Knee Effect

With the incorporation of a P+ region and reduction in the leakage current by deeper junctions, silicon solar cells exhibited significantly higher open circuit voltages and outputs at low temperature and low intensity. However, the frequent presence of a "broken knee" effect was another problem which limited cell efficiency. This effect, when severe enough, could even be observed at high intensity. Figure 9 shows cells which exhibit varying degrees of this effect; beginning at .2 to .4V the cell current falls off sharply with increasing voltage. The reduction in power can be as small as 1-2% or as large as 50 to 75%.

2.2.3.1 Isolation of Causes: I, Series Resistance

Originally, series resistance limited regions in the cell were considered to be responsible for this "broken knee" effect due to the resemblance to the curve shape of cells with reduced area back contacts. Cells with the reduced area back contacts showed a similar looking "distorted knee" effect even when measured at 28°C. In these cases 9% reduction in back contact area at 28°C caused curve distortion, so it was proposed that the standard back contact with the picture frame design could cause the "distorted knee" effect at low temperature and low intensity.

In order to test this explanation, the contact area was reduced by etching off 5 to 80% of the back contact on a group of cells. A curve shape change which resembled the broken knee

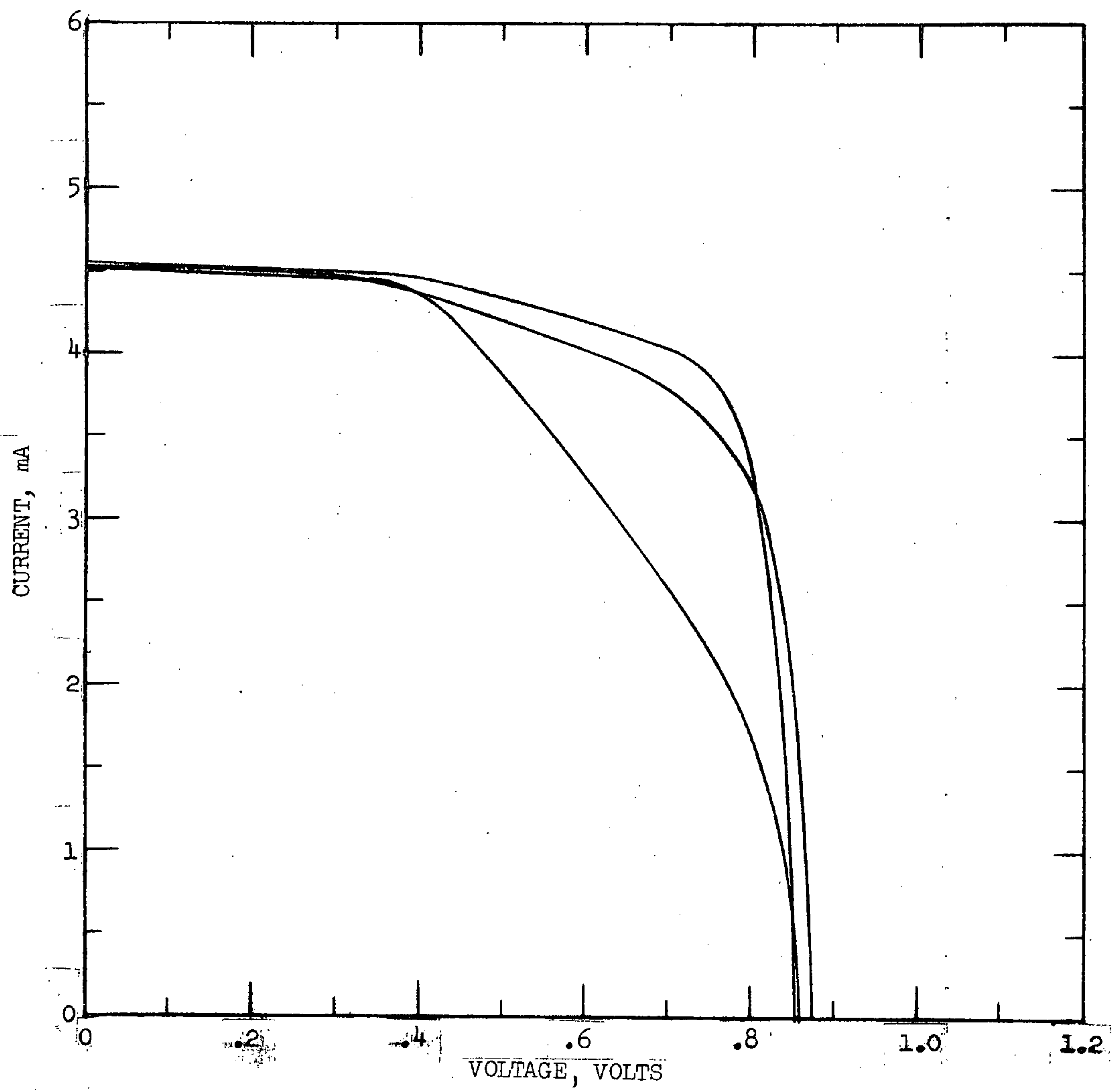

Figure 9. P+ Cells with Various Degrees of the "Distorted Knee" Effect. Measured at -135°C and 5.0 mW/cm^2 AMO in solar simulator.

effect was observed, and it became more pronounced as the contact area was reduced. Though it was similar to the broken knee effect, it occurred in the third quadrant rather than the fourth, and at AMO intensities and 28°C rather than low intensity and low temperature.

Measurements at high intensity showed that as the temperature decreased, the break in the curve shifted into the fourth quadrant and became less apparent. At low intensity and low temperature the broken knee effect, if present originally, was not sigificantly changed and, if absent, was not induced by reduction of the back contact area. This indicated that the broken knee effect observed at low temperature and low intensity could not be explained by a series resistance limited portion of the cell.

2.2.3.2 Isolation of Causes: II, Dependence Upon Location

In order to determine whether the broken knee effect was a uniform defect found in all regions of the cell or caused by localized defects, cells were broken and pieces were measured electrically. Initial measurements showed that pieces with the smallest percentage of bar contact exhibited a less pronounced broken knee. Additional measurements on ~15 cells broken such that part of the cell had just grid lines and the other part had the bar contact showed that cell sections without the bar contact exhibited substantial improvements in fill factor, open circuit voltage, and efficiency. The broken knee was even more pronounced on the cell section with the bar contact than it was on the whole cell. Figure 10 shows I-V curves for a typical cell measured before and after breaking. Table II lists the maximum power, open circuit voltage, curve factor, and efficiency for this same cell. The efficiency (measured in a tungsten light source) of the section of the cell without the bar contact, 17.4%, was double the unbroken cell efficiency of 8.7%.

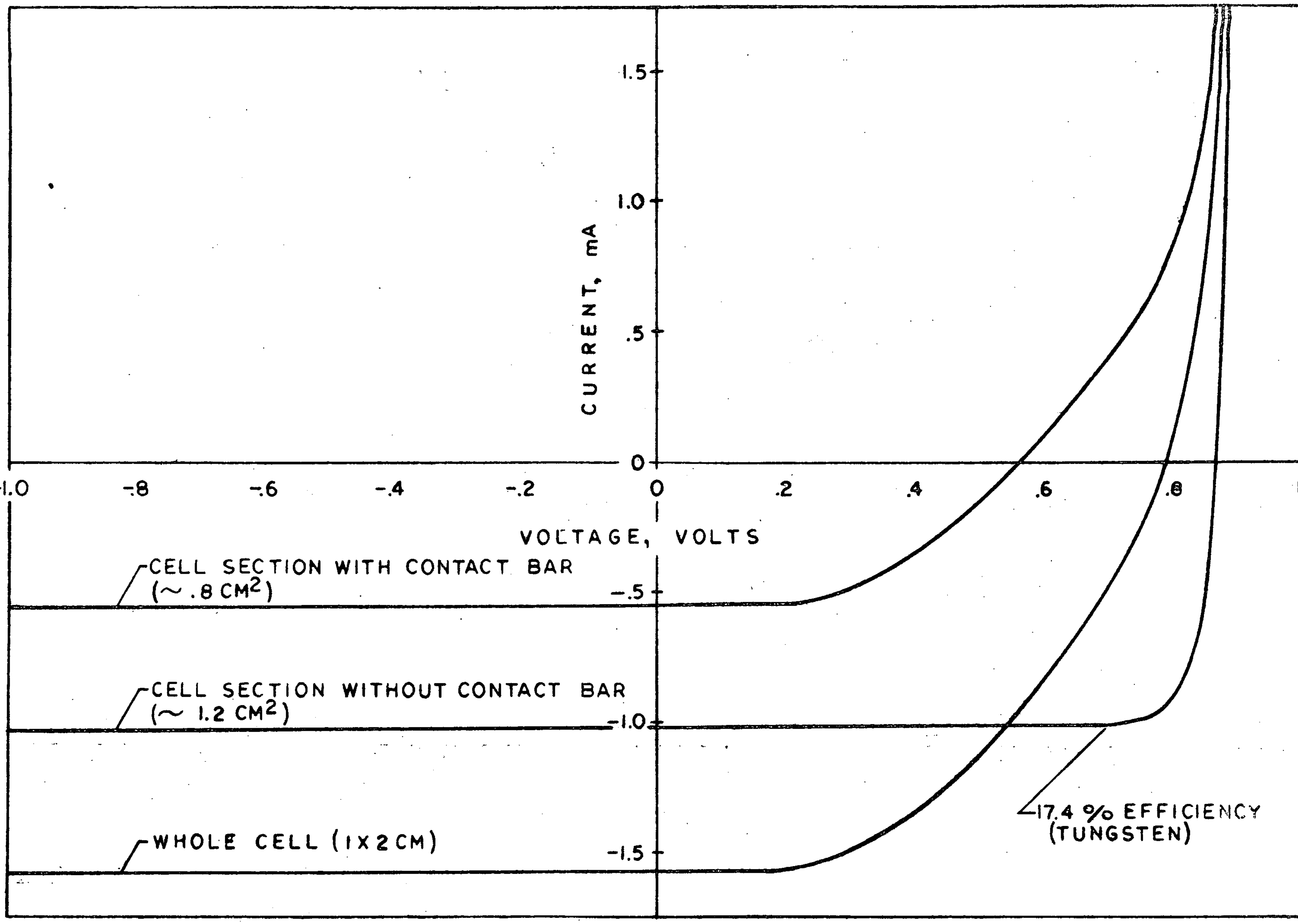

Figure 10 **I-V Characteristic Curves of a "Broken Knee" Cell. 10 ohm cm Float Zone N/P P+ Cell measured in a tungsten light source, 3.58 mW/cm^2, -135°C.**

TABLE II

Electrical Characteristics of a "Broken Knee" Cell

Cell Description	P_{Max} mW	V_{oc} Volts	C.F.	Efficiency* %
1. Whole cell	.56 at .50V	.790	.452	8.7
2. Section with Bar	.15 at .35V	.560	.484	6.8
3. Section without Bar	.74 at .76V	.865	.842	17.4

*Based upon cell measurements obtained at -135°C under a tungsten light source set to 100 mW/cm^2 and then neutrally filtered to 3.58 mW/cm^2.

This same type of effect was observed with cells having only slightly reduced output due to a soft knee. A cell having an initial efficiency of 16% (measured in a tungsten light source) and a curve factor of 0.776 was broken and the cell section without the bar contact had an efficiency of 16.8% and a curve factor of .814.

A possible explanation for the efficiency improvement in cell sections without the bar contact, with the bar contact section exhibiting even lower efficiency than the whole cell is:

1. The cell section with the bar has a much greater amount of metal which could fire into the junction in the sintering operation, or

2. The cell section with the bar has a large amount of metal near the cell edge; on the other section the grid lines are not even near the edge.

In either case, the probability of current leakage paths would be greater on the bar contact section of the cell and to some extent, the effect of the broken knee phenomenon on the I-V curve does resemble a leakage path.

2.2.3.3 Investigation of Edge Treatments

In order to determine whether the broken knee effect was related to leakage paths at the cell edges, various techniques for altering the cell edges were used and their effects, if any, on the I-V characteristic curve were analyzed. These procedures included:

1. Etching the silicon slabs prior to slicing to reduce the mechanical damage which would be present on the cell edges,

2. Grinding cell edges after fabrication,

3. Application of a liquid glass film which was then heated to between 400 and 600°C to form a passivating layer,

4. Investigation of various post-fabrication etching techniques.

It is well known that silicon is mechanically damaged during the cutting operations. In order to reduce the amount of damage which might still be present at the cell edges even after the prediffusion etch, an additional etch was used to remove 0.005 inch (125 μM) of silicon from all surfaces of silicon slabs prior to their being sliced into blanks. Both Mon-X and crucible grown silicon slabs were processed in this manner and experimental Jupiter type solar cells were fabricated from the material. Measurement of the I-V characteristic curves at -135°C in both simulator and tungsten light sources showed that although the broken knee effect was not completely eliminated, the problem was reduced.

Only one out of ten of the cells had an efficiency of less than 13% (X-25 Solar Simulator). The other cells had efficiencies ranging from 13.8 to 15.2% (See Figure 11). Since previous groups of cells have frequently shown less than 50% yield of cells with efficiencies of 13% or more, this etching procedure was an improvement.

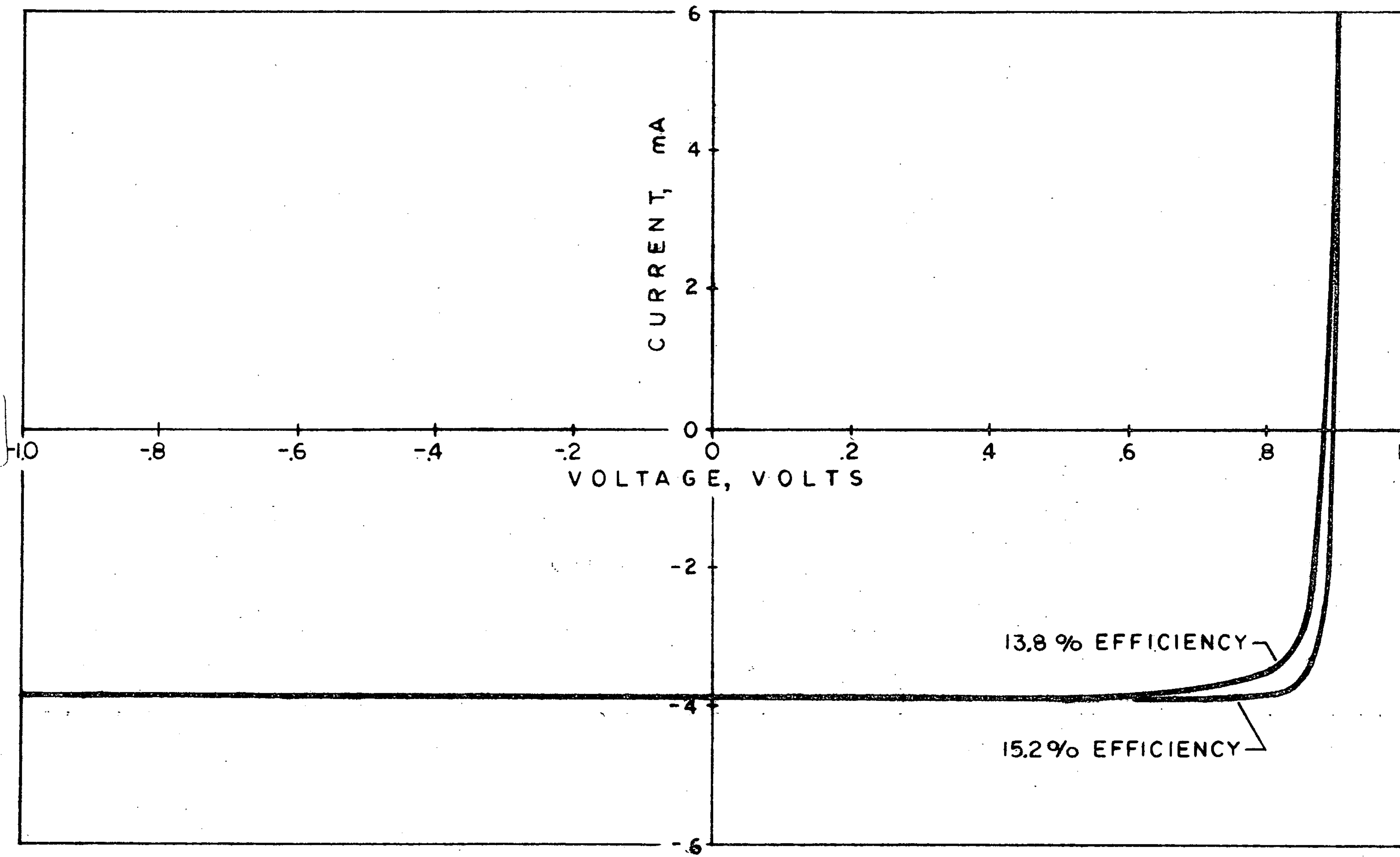

Figure 11. I-V Characteristic Curves of Mon-X Cells Measured at 5.0 mW/cm^2 Solar Intensity and -135°C.

Grinding the cell edges was also investigated for its effects upon the broken knee characteristics since this treatment should mechanically alter the surface states. Frequently the edges of cells with the broken knee characteristics show mechanically damaged regions when inspected under a microscope (40 X magnification). Grinding the cell edges with 3M Co. #600 abrasive lapping paper to remove the damage regions produced varying results; (additional polishing on finer grit paper did not improve the cell characteristic curve).

Figure 12 shows curves measured at -135°C in a tungsten light source (3.58 mW/cm^2 intensity) before and after grinding the edges of a 1 x 2 cm cell (no AR coating). With this particular cell the extreme broken knee of the cell as fabricated was completely removed merely by grinding all four cell edges. This procedure, however, as a general rule did not always completely remove the problem; for the majority of the cells it merely reduced the problem. For example, Figure 13 shows I-V characteristic curves (measured under the same conditions as those mentioned above) of a cell before and after grinding one edge and then four edges. Grinding just one edge which had a damaged region reduced the broken knee considerably, but it was still present. Grinding the other three edges did not produce any further improvement.

Figure 14 shows an even more extreme example of the broken knee. It was also reduced considerably, but not eliminated by grinding one of the edges. The other three edges were also ground, but no further improvement was observed.

A third technique investigated for its effects on the broken knee characteristics involved applying a suspension of glass in a liquid to the cell edges and then heating it to 400 to 600°C to harden it. This procedure did eliminate the broken knee effect on some of the cells on which the edges had been ground prior to application of the glass film. None of the cells with unground edges showed any

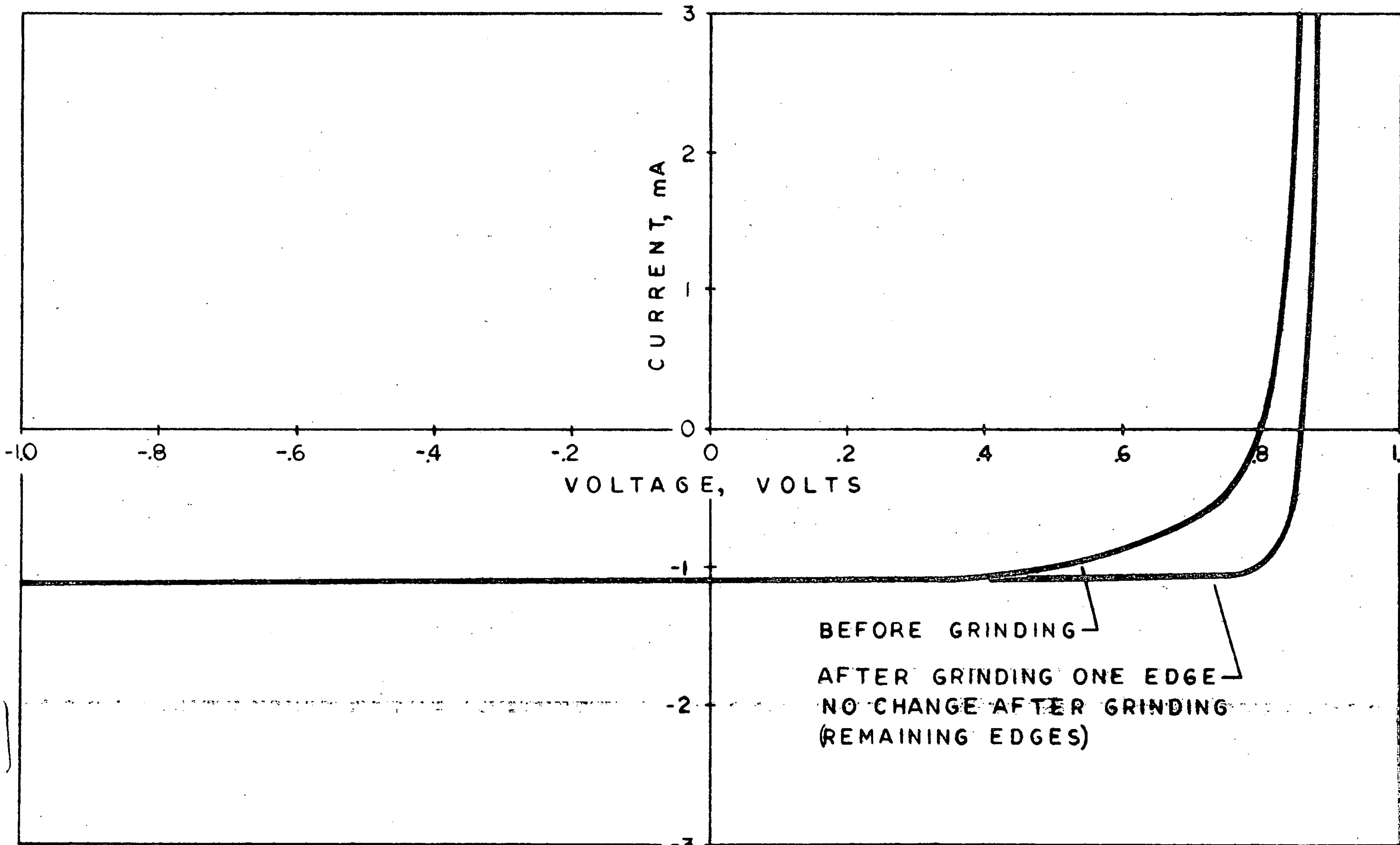

Figure 12. **Effect of Grinding Cell Edges on Broken Knee Characteristic.**
1 x 2 cm cell measured at -135°C in a tungsten light source at 3.58 mW/cm^2 intensity.

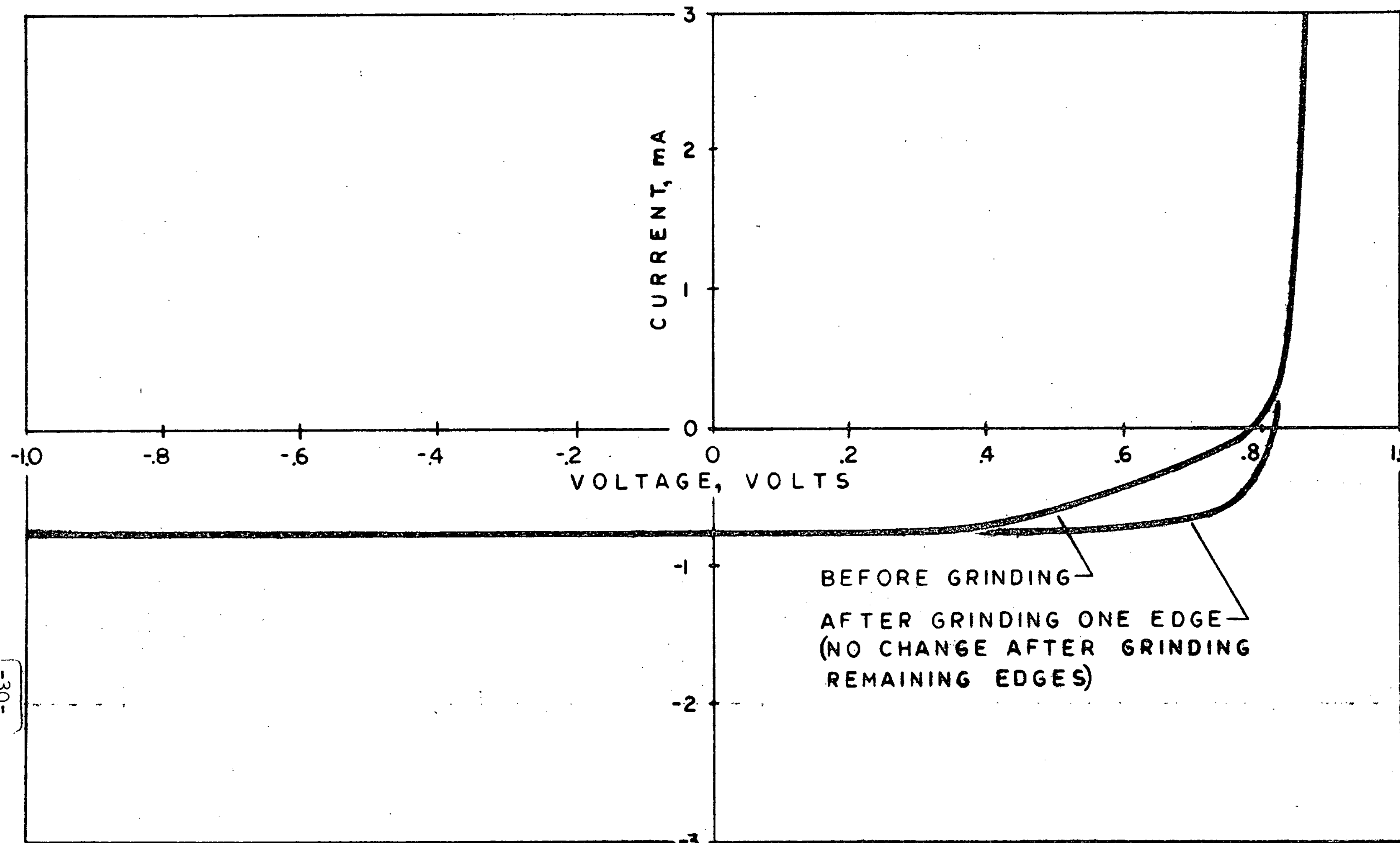

Figure 13. Effect of Grinding Cell Edges on Broken Knee Characteristic. 1 x 2 cm cell measured at -135°C in a tungsten light source at 3.58 mW/cm^2 intensity.

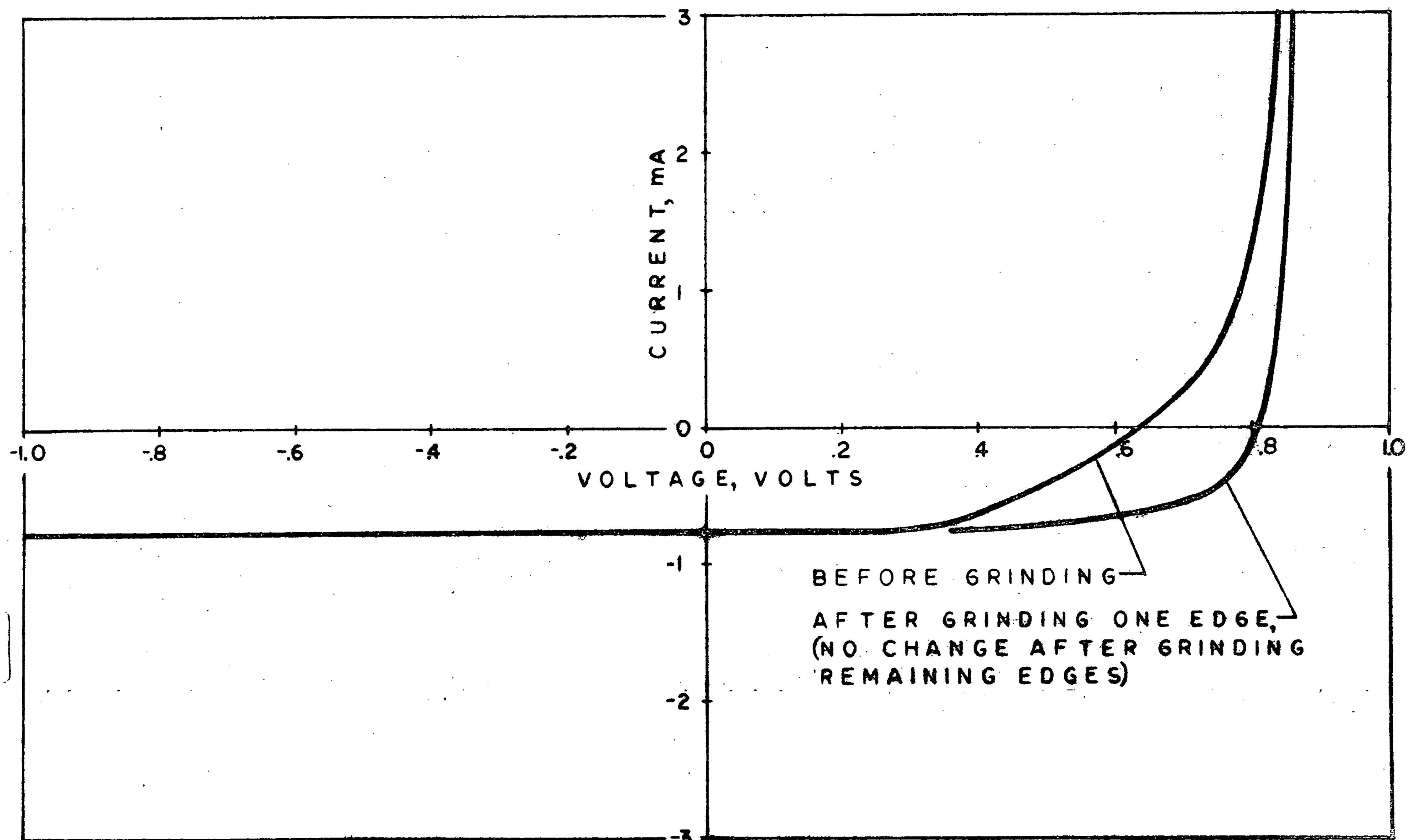

Figure 14. Effect of Grinding Cell Edges on Broken Knee Characteristic.
1 x 2 cm cell measured at -135°C in a tungsten light source
at 3.58 mW/cm^2 intensity.

significant improvement and the number of cell edges ground was found to affect the improvement. Figure 15 shows the effect of the glass layer after application to the same cell which was shown in Figure 13. The broken knee effect which was reduced by grinding the cell edges was completely eliminated after application of the glass film.

Two basic post-fabrication etching techniques were investigated:

1. A mesa etch which involves etching the cell edges and a narrow region from the perimeter of the top surface of the cell, and
2. Etching only the cell edges.

The mesa etch moves the junction edge away from the cell and minimizes the contamination which might otherwise occur at the junction edge. A number of conventional cells (without a P^+ region on the cell back surface) were fabricated with this mesa etching technique and measured. Even with the Schottky barrier present these cells did provide useful information on the broken knee problem since broken knee break-down usually occurs at .3 to .4V and the Schottky barrier only affected the cell I-V characteristic curve beyond .6 to .65V. Measurement of these cells at -135°C in a tungsten light source (intensity of 3.58 mW/cm^2) indicated that mesa etching might be a valuable procedure to incorporate into the fabrication process for a Jupiter type cell. Only four out of sixteen devices measured exhibited a broken knee effect and in each case the effect was not a serious as is frequently seen with cells processed according to standard techniques being used for P^+ cells.

For edge etching, tape, trimmed away from the cell edges, was used as a mask for the cell surfaces. Two acid mixtures were used: a 2-3 HNO_3 -HF mixture (fast etching) and a 5-3-3 HNO_3 -HF-HAc mixture (CP-4A, slower etching). Etching time in both cases was ~10 seconds.

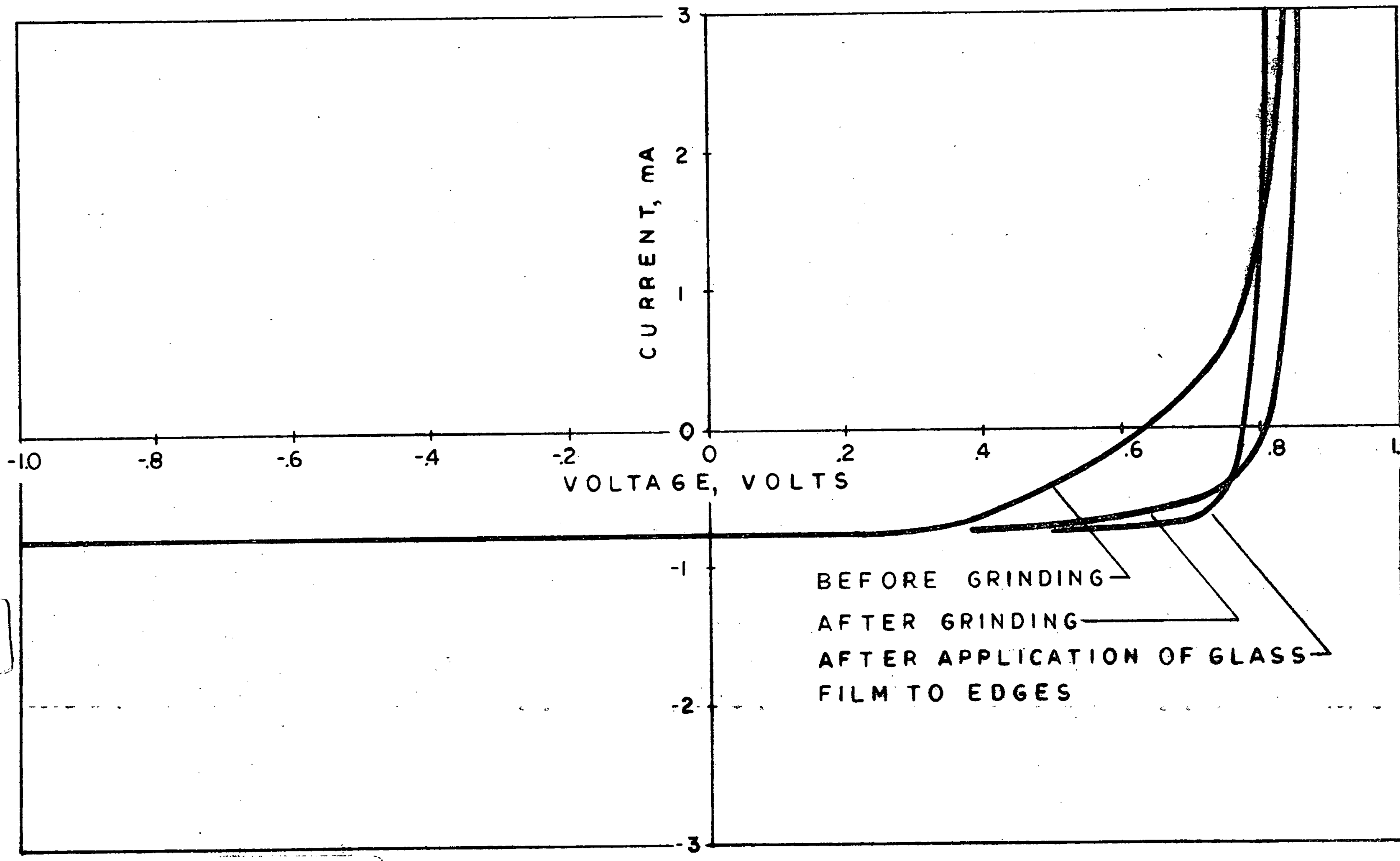

Figure 15. Effect of Applying Glass Film to Cell with Ground Edges.
1 x 2 cm cell measured at -135°C in a tungsten light source
at 3.58 mW/cm^2 intensity.

Although the fast etching acid was effective in eliminating leakage paths caused by metal contamination on the junction edge, neither mixture eliminated the broken knee effect. Increasing the time to 2-3 minutes in the CP-4A etch reduced the broken knee effect, but the improvement was masked now by a soft or rounded knee. Soaking cells in HNO_3 for 2-3 minutes after the CP-4A etch minimized the rounded knee effect. From this work we learned that it was necessary to remove several mils of silicon to produce a major improvement in output. This fact was reinforced during the pilot production phase. In some cases, due either to accidental reduction in the etching time or etch rate, less than .001" was removed from the cell dimensions. This produced only a slight modification in the broken knee effect, and a second edge etch was necessary to improve the cell output significantly.

The etching procedure finally used reduced overall cell dimensions .002 to .003" and included the following steps:

1. HNO_3 dip - 15 sec.

2. CP-4A etch - 3 min.

3. HNO_3 soak - 2 min.

2.2.3.4 Conclusions

A sharp decrease in current starting between .2 and .4V, which has been called a "broken knee" effect, can reduce cell output at low temperatures and low intensity by as much as 50 to 75%. Breaking solar cells and measuring the I-V curves of various pieces showed that this broken knee characteristic could be correlated to that region of the cell with the bar contact. Further investigation pinpointed the problem to the cell edges in the bar contact region. An edge etching procedure has been developed which reduces this broken knee effect to the extent that a high yield of cells with 14% efficiency or better can be obtained.

2.2.4 Short Circuit Current Effects vs. Temperature

Another problem which seriously reduced cell efficiency was large variations in the thermal coefficient of short circuit current. The short circuit current versus temperature relationship is usually nonlinear, and in many cases the short circuit current decreases sharply between -60° and -120°C (Figure 16).

The short circuit current effect occurs at both high and low intensities and is not dependent upon initial short circuit current at 140 mW/cm^2. The magnitude of this effect is illustrated in Figure 17. I-V curves (measured in an X-25 solar simulator) of three different cells are compared at low temperature and 5.0 mW/cm^2 intensity. The cell with the broken knee has the highest efficiency (15.2%) because the short circuit current decreased linearly with temperature. The efficiencies of the other two cells were lower (14.4 and 12.9%) because the short circuit current decreased sharply between -60 and -120°C. Thus, even though the cell with the broken knee had a poor curve factor, it had higher output since the severe reduction in short circuit current limited the output of the other two cells.

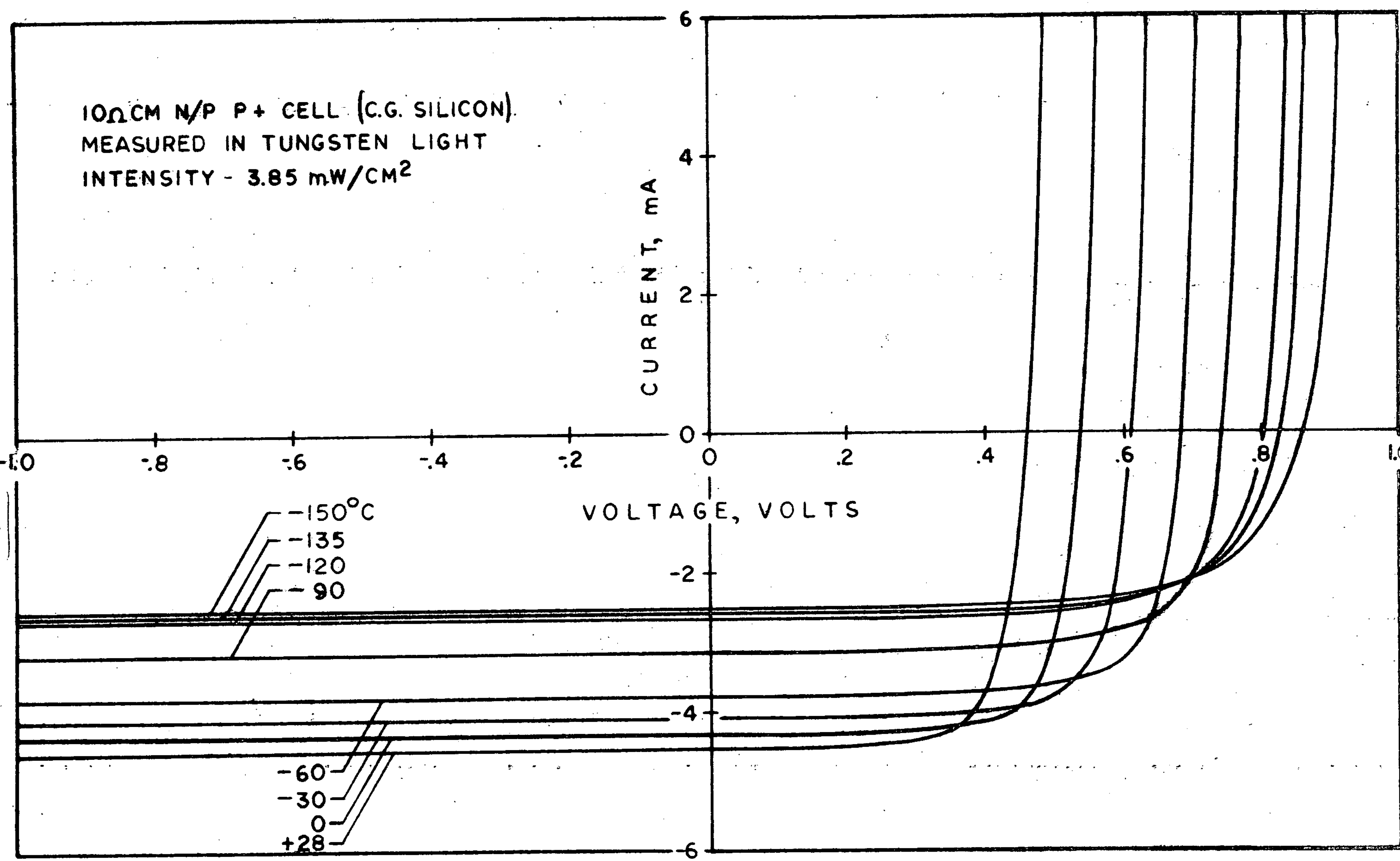

Figure 16. Cell with Low Isc at -135°C Due to Increase in ΔIsc/ΔT

38½%

8

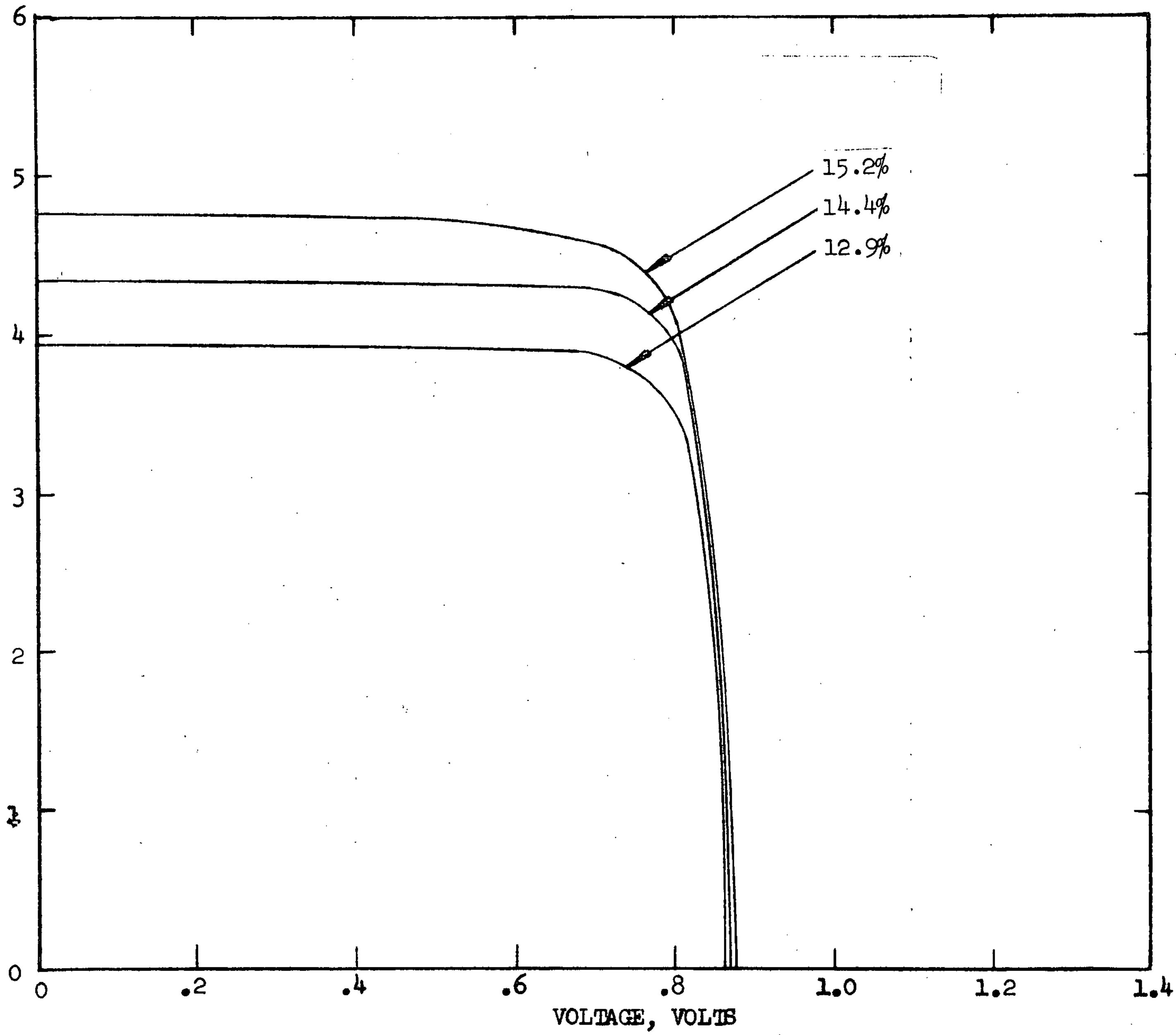

Figure 17. Output of 10 ohm cm N/P Cells with P+ Region. Measured at $5.0\ mW/cm^2$ AMO in X-25 Solar Simulator at -135°C.

2.2.4.1 Influence of Silicon Growth Technique: Float Zone and Mon-X vs. Crucible Grown

Comparison of P+ cells fabricated from silicon made by the float zone growing technique (low oxygen content and high dislocation density) and Mon-X growing technique (low oxygen content and low dislocation density) to P+ cells fabricated from crucible grown silicon showed that the Mon-X and float zone cells exhibited a short circuit current vs. temperature dependence which was more linear.

In Figure 18, two solid lines describe the short circuit current versus temperature relationship for the float zone cells with the highest and lowest I_{sc} temperature coefficients, and the two dashed lines describe the same for the Mon-X cells. The short circuit current for the best float zone cell decreased linearly with only .37 mA change between +28 and -135°C. This represents a change of 8% from initial current. The float zone cell with the largest change in short circuit current over this temperature range was .67mA; this was approximately 15% lower than the initial value for short circuit current.

The curves in Figure 19 show short circuit current versus temperature for crucible grown P+ cells. The range of short circuit currents is shown at both -135 and 28°C. Curves A and C exhibit minimum fall off in short circuit current, 15 to 17% from the initial value, while Curve E shows the greatest change, 30%, for this group of 24 cells.

The oxygen concentration, 10^{14} and 10^{15} atoms/cm^3 for float zone and Mon-X silicon, compared to 10^{17} to 10^{18} atoms/cm^3 for crucible grown silicon, was assumed to be responsible for the improvement in the short circuit current vs. temperature relationship of float zone and Mon-X cells. This theory is not invalidated by the occasional observation of this linear behavior in crucible grown

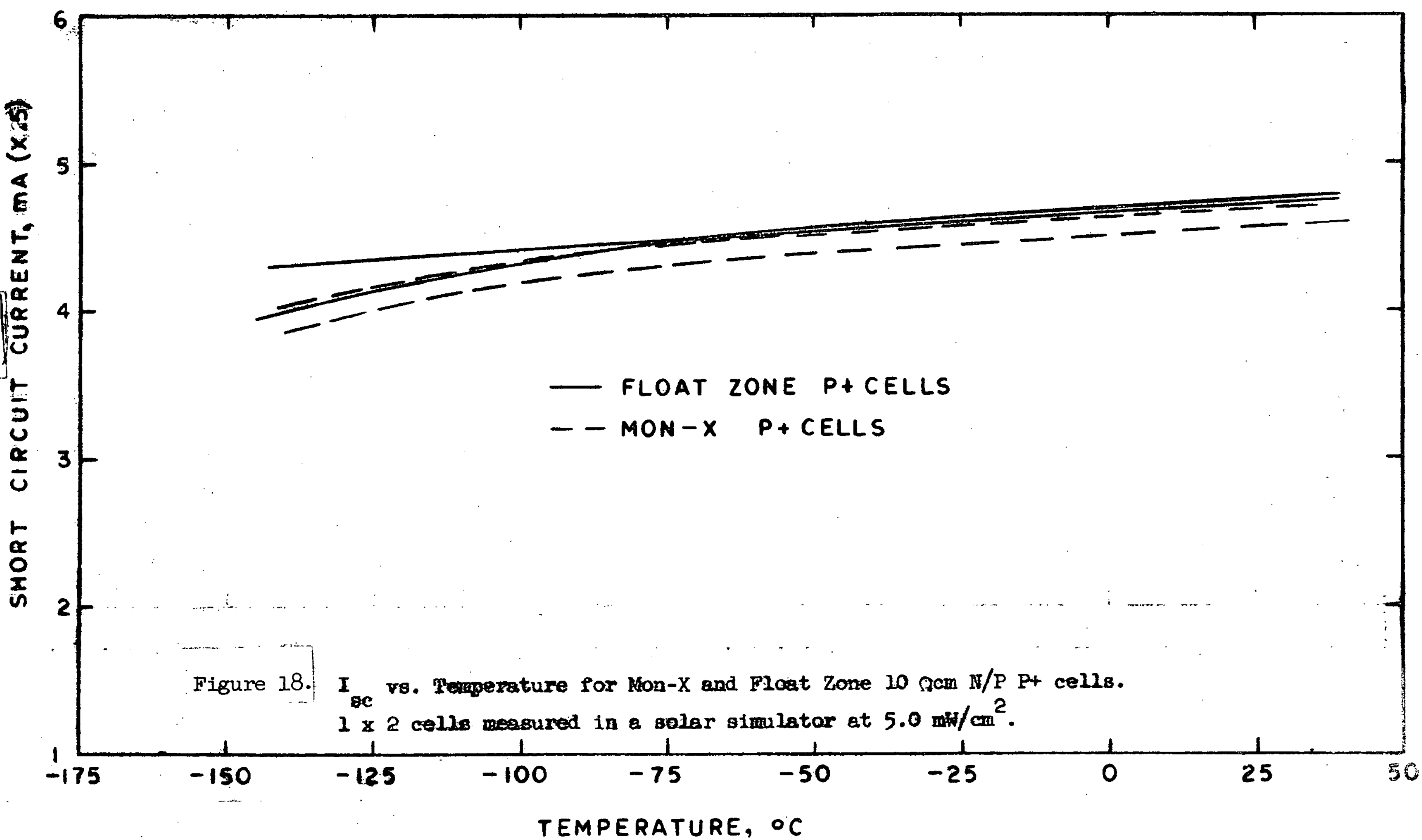

Figure 18. I_{sc} vs. Temperature for Mon-X and Float Zone 10 Ωcm N/P P+ cells. 1 x 2 cells measured in a solar simulator at 5.0 mW/cm^2.

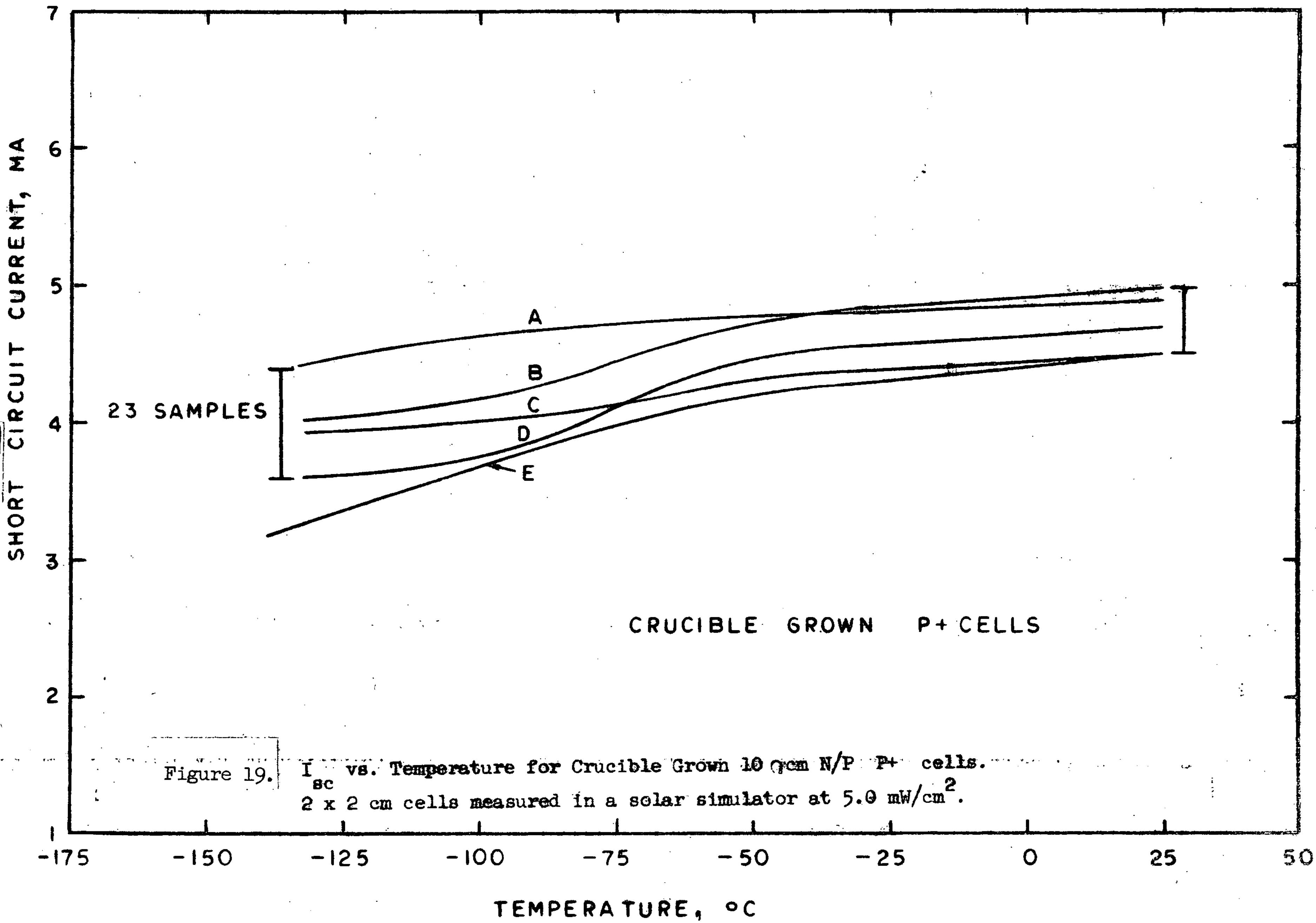

Figure 19. I_{sc} vs. Temperature for Crucible Grown 10 Ωcm N/P P+ cells.
2 x 2 cm cells measured in a solar simulator at 5.0 mW/cm^2.

silicon cells. Oxygen concentration is known to vary along the length as well as across the diameter of an ingot of crucible grown silicon. The oxygen concentration also changes with crystal and crucible rotation which is varied during the growing procedure.[7)]

2.2.4.2 Variations in Growing Parameters of Crucible Grown Silicon

An experiment was performed to determine whether the improved low temperature short circuit current could be duplicated with crucible grown silicon. Although crucible grown silicon cannot be grown with the very low oxygen concentration found in float zone silicon, approximately an order of magnitude reduction to 10^{17} atom/cm^3 can be obtained by reducing the crucible rotation and the ingot diameter. A special ingot was grown with low crucible rotation and a diameter of 1.25 to 1.50 inches rather than the typical ingot diameter of 2.0 to 2.5".

When the ingot was cut, the top, center and bottom sections were kept separate and identified so that any differences in the cell characteristics as a function of position in the ingot could be observed, since each section should have a different amount of oxygen dissolved in it. For comparison a standard production ingot was also cut with top, center and bottom sections kept separate.

Solar cells made from each section of the ingot were measured between 28 and -135°C in a tungsten light source (3.58 mW/cm^2 intensity). None of the sections from either ingot produced cells with an improved short circuit current versus temperature dependence. The cells from the standard production ingot (used as a control) showed a 12 to 28% deviation from the linearly extrapolated values. The cells from the top section of the lower oxygen content ingot showed 25 to 35% deviation and the cells from the middle sections 19 to 22% deviation from linearity. In the case of the cells fabricated from the bottom section of the ingot grown to minimize oxygen content, the short circuit current measured in a tungsten light source at 28°C was 40 to 50 mA rather than 110 to 120 mA and the short circuit current decreased sharply with temperature between 28 and -60°C rather than between -60 and -120°C which is the range in which the short circuit current usually deviates from a linear relationship. Since the growing parameters which were modified were the most significant ones with respect to altering the oxygen concentration, it was concluded that the oxygen concentration of crucible grown silicon could not be altered enough to improve the short circuit current versus temperature relationship.

2.2.4.3 Effects of Diffusion Changes

Changes in the junction depth also influenced $\Delta I_{sc}/\Delta T$. Under an AMO spectrum, the I_{sc} decreases as the junction depth increases. For example, increasing the junction depth from 0.5 to 1.0μM decreased the I_{sc} ~8% from ~135 to ~125mA, or at low intensity from 4.90 to 4.46 mA. At -135°C however, the cells with junction depths of 1.0μM had short circuit currents only 1 to 2% lower, due to lower $\Delta I_{sc}/\Delta T$, than cells with shallower junctions. As mentioned in Section 2.2, going from a junction depth of 0.5μ to 1.0μ resulted in a leakage current reduction of ~25%. The improvement in curve factor combined with only 1 to 2% lower I_{sc} produced a net gain in output.

2.2.4.4 Conclusions

The wide range in short circuit current at -135°C observed with crucible grown silicon due to variations in $\Delta I_{sc}/\Delta T$ can be reduced by using low oxygen, low dislocation density silicon such as Mon-X or Lopex. In addition $\Delta I_{sc}/\Delta T$ decreases with increasing junction depth. This means that the junction depth can be increased to reduce leakage current without sacrificing proportionately as much current at -135°C as at 28°C.

2.3 A QUICK METHOD FOR PRE-SELECTING CELLS OF ADEQUATE EFFICIENCY UNDER SIMULATED JUPITER CONDITIONS

Measurement of cells at -135°C in the dark as well as at 5.0 mW/cm^2 intensity has shown that the dark forward I-V characteristic curve duplicates the shape of the low intensity I-V characteristic curve (Figure 20). Although a dark measurement is more convenient than a measurement at a specific intensity, it is the low temperature aspect which makes the testing time-consuming and expensive. What was needed was a correlation between the I-V characteristic curve at -135°C either in the dark or at low intensity and the I-V characteristic curve at a more convenient temperature. With the broken knee effect being a low temperature occurrence, a room temperature measurement could not be used, and consequently, -196°C (LN_2 temperature) was selected.

If a correlation between the -196°C and -135°C measurements could be established, the dark measurement at -196°C could be used by itself to pre-select cells for testing at 5.0 mW/cm^2 solar intensity and -135°C, or it could be used as part of the following sequence to indicate cells of particular efficiency or better.

1. Determination of $\Delta I_{sc}/\Delta T$ on a simple basis
2. Measurement of I_{sc} of all cells at 28°C
3. Measurement of all cells at -196°C

These tests are described in detail in the following sections and examples are shown in Figure 21.

2.3.1 Determination of $\Delta I_{sc}/\Delta T$ on a Sample Basis

The change in I_{sc} between 28°C and -135°C at 5.0 mW/cm^2 intensity

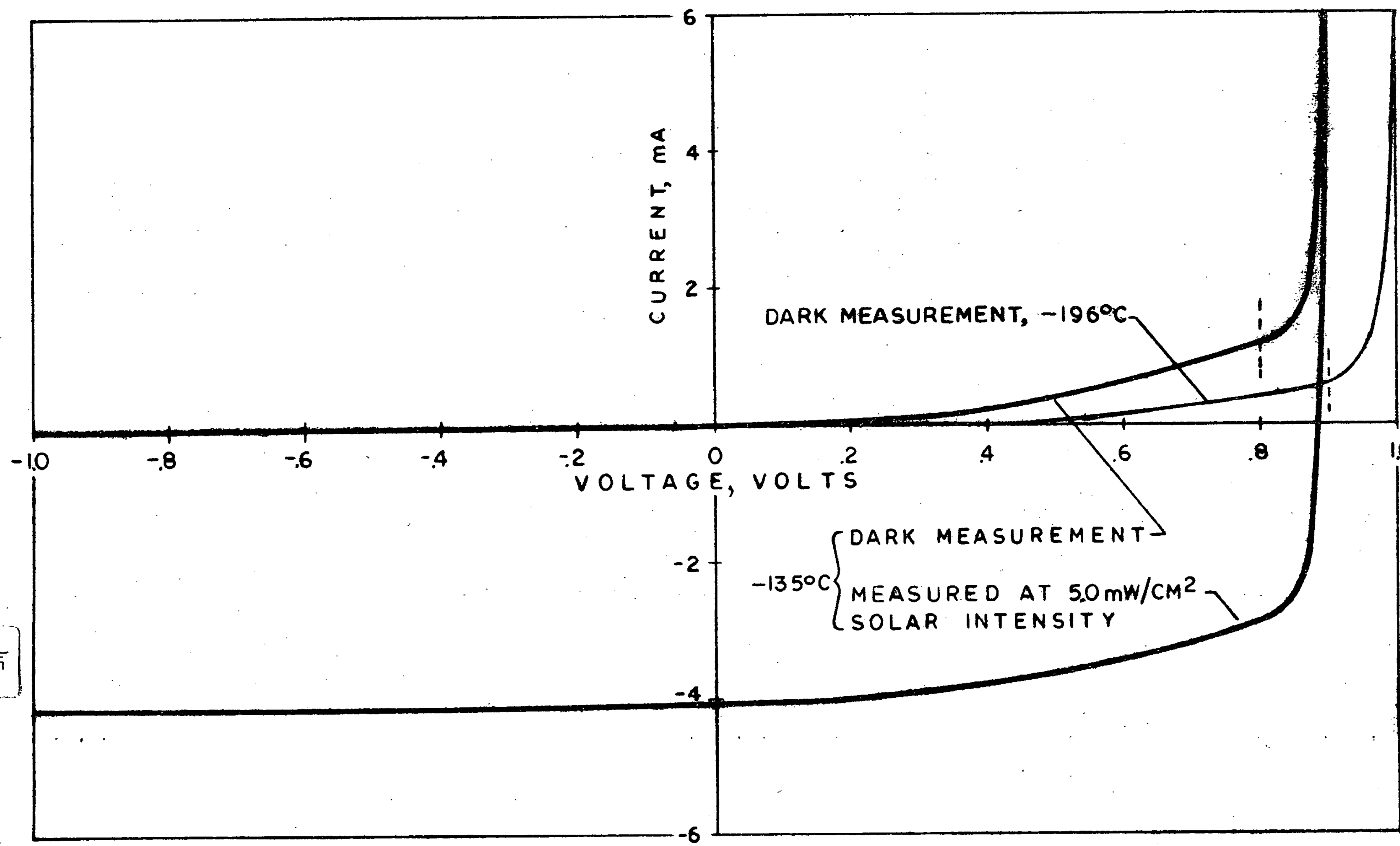

Figure 20 Comparison of Dark and Low Intensity Measurements

has been observed to range from .25 to .7 mA for Mon-X and Lopex silicon; that is, if the I_{sc} at 28°C was 4.5 mA, the I_{sc} at -135°C would be between 3.8 and 4.25 mA. The $\Delta I_{sc}/\Delta T$ is dependent upon growth technique and diffusion parameters. For example Mon-X and Lopex silicon exhibit consistently lower thermal coefficients than crucible grown silicon. Increasing the junction depth also decreases $\Delta I_{sc}/\Delta T$. A shallow junction of $\sim$.5 μM produces a current reduction of .6 to .7 mA, whereas a junction depth of ~1.0 μM results in a current reduction of .3 to .4 mA. Increasing the junction depth further decreases $\Delta I_{sc}/\Delta T$. Consequently, determination of $\Delta I_{sc}/\Delta T$ on a sample basis would be advisable in terms of production control since shifts in $\Delta I_{sc}/\Delta T$ would indicate variations or problems in the diffusion process or the initial silicon characteristics. In addition, if the maximum change is .4 mA rather than .7 mA, lower I_{sc} at 28°C can then be acceptable.

2.3.2 Measurement of I_{sc} of All Cells at 28°C

The measured $\Delta I_{sc}/\Delta T$ can be used with a measurement of I_{sc} at 28°C to calculate the I_{sc} at -135°C, 5.0 mW/cm^2 solar intensity. (See A through C, Figure 21.) The I_{sc} at 28°C could be measured either at 140 or 5 mW/cm^2, whichever was more convenient. If cells were measured at 140 mW/cm^2, it would be a simple matter to calculate I_{sc} at 5.0 mW/cm^2, since I_{sc} is directly proportional to the light intensity.

2.3.3 Dark Measurement in LN_2

As mentioned previously the dark I-V curve measured at -135°C duplicates the curve shape obtained at 5.0 mW/cm^2. Correlation of -135°C measurements to more easily obtained LN_2 (196°C) dark measurements would make it possible to pre-select cells for testing at -135°C and 5.0 mW/cm^2 solar intensity or, if the above measurements (Sections 2.3.1, 2.3.2) were made, to establish the efficiency range under Jupiter conditions.

Comparison of the dark current measured at .9V at -196°C to the change in current from short circuit to .8V ($\sim P_{max}$) made it possible to establish the relationships shown in Table III. Table III also shows the efficiency calculated using 4.0 mA as a typical short circuit current at 5.0 mW/cm^2, -135°C. The efficiency is determined in the following manner. If the current at .9V is between .1 and .2 mA (Group III), the ΔI (I_{sc}-I at .8V) at -135°C is .3-.5 mA. Using 4.0 mA as the I_{sc} this means the current at P_{max} (.8V) would be no lower than 3.5 mA, corresponding to a minimum output of 2.8 mW or an efficiency of 14 percent (based upon 4 cm^2). The Group I and II relationships could be used for classifying cells into higher minimum efficiency groups (see Table III) or as cut-off points for cells with short circuit currents lower than 4.0 mA.

Table III

Dark, -196°C vs. 5.0 mW/cm^2, -135°C Measurements

Group	Dark, -196°C I at .9V, mA	5.0 mW/cm^2, -135°C $\Delta I = I_{sc}$-I at .8V	Calculated Minimum(1) Effic. Using 4.0 mA(2) as I_{sc} at -135°C
I	0 - .01	0 - .1	15.6%
II	.01 - .1	.1 - .3	14.8%
III	.1 - .2	.3 - .5	14.0%

(1) Minimum because the largest ΔI in each category is used in calculating efficiency.

(2) 4.0 mA is used for convenience; actual values in pilot production ranged from 3.7 to 4.4 mA.

The following is an example of calculating cell efficiency according to the method shown in Figure 21; a specific cell from Lot 3 (352-1) was used.

	Method	Results
A.	Using a sample of 10 cells the ΔI_{sc} at 5.0 mW/cm^2 between 28 and -135°C was determined.	.3 - .4 mA
B.	The cell I_{sc} was measured at 5.0 mW/cm^2, 28°C.	4.8 mA
C.	The cell I_{sc} at -135°C was determined by subtracting A from B.	4.4 mA
D.	The dark I was measured at .9V at -196°C.	.1 mA
	Corresponding ΔI at -135°C (from Table III).	.3 mA
	I at .8V = 4.4 - .3 mA	4.1 mA
E.	Calculated output	3.28 mW
F.	Calculated efficiency	16.4%

This was within 1% of the actual measured output (at 5.0 mW/cm^2, -135°C) of 3.31 mW (16.55% efficiency).

Procedure for Determining Cell Efficiency or Output at -135°C, 5.0 mW/cm^2

	Test		Example				
A.	Determine $\Delta I_{sc}/\Delta T$ on sample basis		.3 $\pm$ .1 mA change between 28 and -135°C				
B.	Measure I_{sc} at 140 mW/cm^2, 28°C	Classify cells in I_{sc} groupings	134.3	131.7	128.8	126	123.2
	Calculate I_{sc} at 5.0 mW/cm^2, 28°C		4.8	4.7	4.6	4.5	4.4
C.	Calculate I_{sc} at -135°C on basis of A.		4.4-4.6		4.2-4.4		4.0-4.2
D.	Determine I at .8V (V_{mp}) on basis of -196°C dark measurement of I at .9V and following correlations:	Dark I, mA					
		I <.01	$\geq$4.3-4.5		$\geq$4.1-4.3		$\geq$3.9-4.1
		.01< I $\leq$.1	$\geq$4.1-4.3		$\geq$3.9-4.1		$\geq$3.7-3.9
		.1 < I $\leq$.2	$\geq$3.9-4.1		$\geq$3.7-3.9		$\geq$3.5-3.7
E.	Calculate output		3.44-3.60		3.28-3.44		3.12-3.28
			3.28-3.44		3.12-3.28		2.96-3.12
			3.12-3.28		2.96-3.12		2.80-2.96
					Efficiency, % (4.0 cm^2)		
F.	Calculate efficiency		17.2-18.0		16.4-17.2		15.6-16.4
			16.4-17.2		15.6-16.4		14.8-15.6
			15.6-16.4		14.8-15.6		14.0-14.8

Figure 21

3.0 PILOT PRODUCTION

3.1 FABRICATION PROCEDURE

This program included a pilot production phase in order to demonstrate the ability to fabricate quantities of cells for use in a Jupiter environment and to obtain sufficient statistical data on cell performance. The basic procedure for fabricating N/P solar cells was used, but with several process additions and modifications to obtain improved low temperature and low intensity performance. Figure 22 is a flow chart showing the basic fabrication steps as well as the quality control check points. The steps which have been added or changed are indicated; they include:

1. etching slabs prior to slicing in order to reduce mechanical damage on cell surfaces which will become cell edges,

2. 2-hour rather than 32-minute diffusion to obtain lower leakage currents,

3. Al evaporation prior to TiAg evaporation to obtain contacts which are ohmic at low temperature,

4. edge etching to reduce leakage effects.

Cells were measured in the dark at -196°C prior to soldering, since edge etching, if necessary for elimination of leakage paths, must be done before soldering. The cells were measured again after edge etching to evaluate the degree of improvement. The cells were then soldered, inspected for mechanical defects, and electrically tested at 5.0 mW/cm^2 solar intensity and -135°C.

CRYSTAL AND MECHANICAL PROCESSING

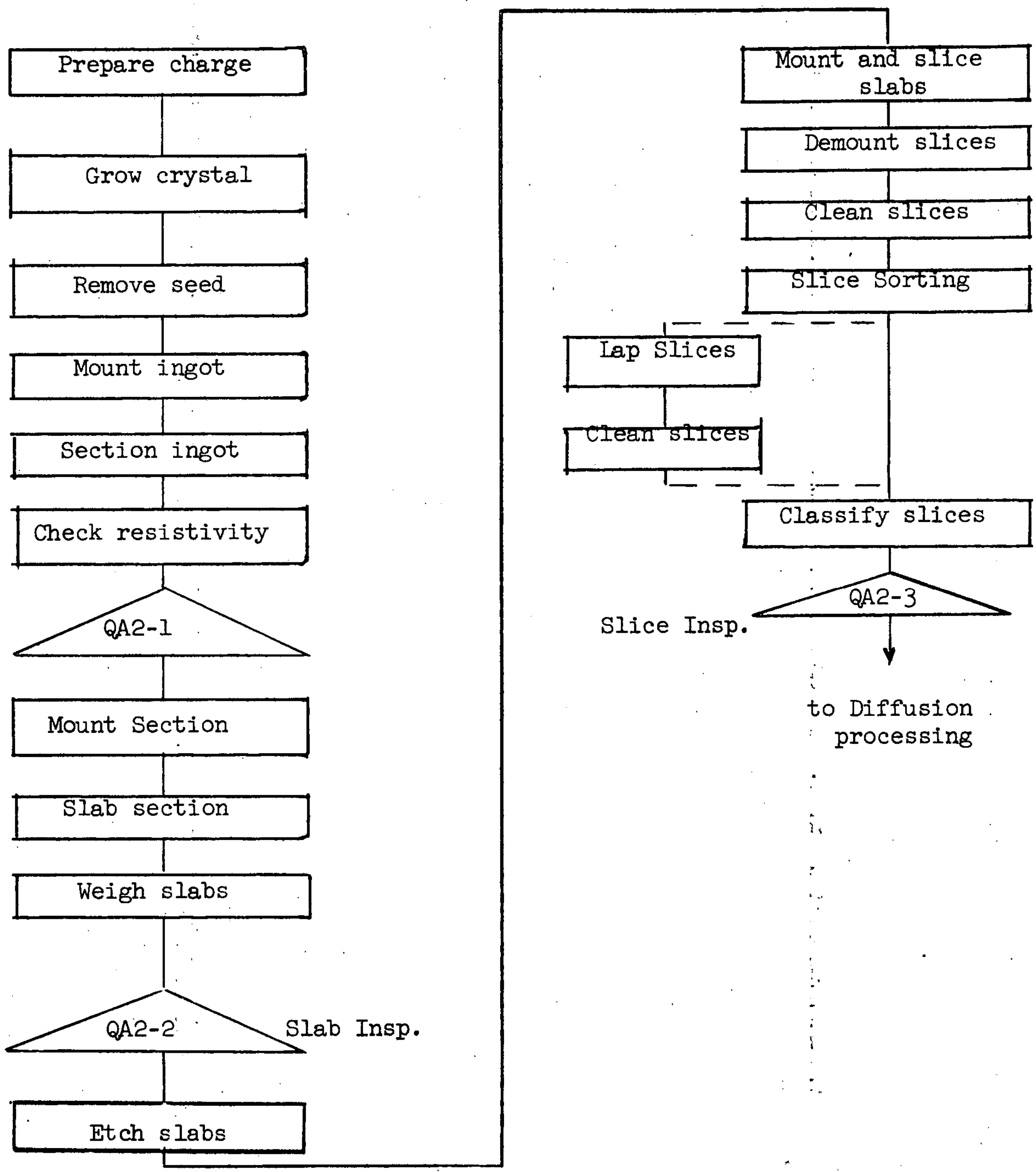

Fig. 22a

DIFFUSION AND FINAL PROCESSING

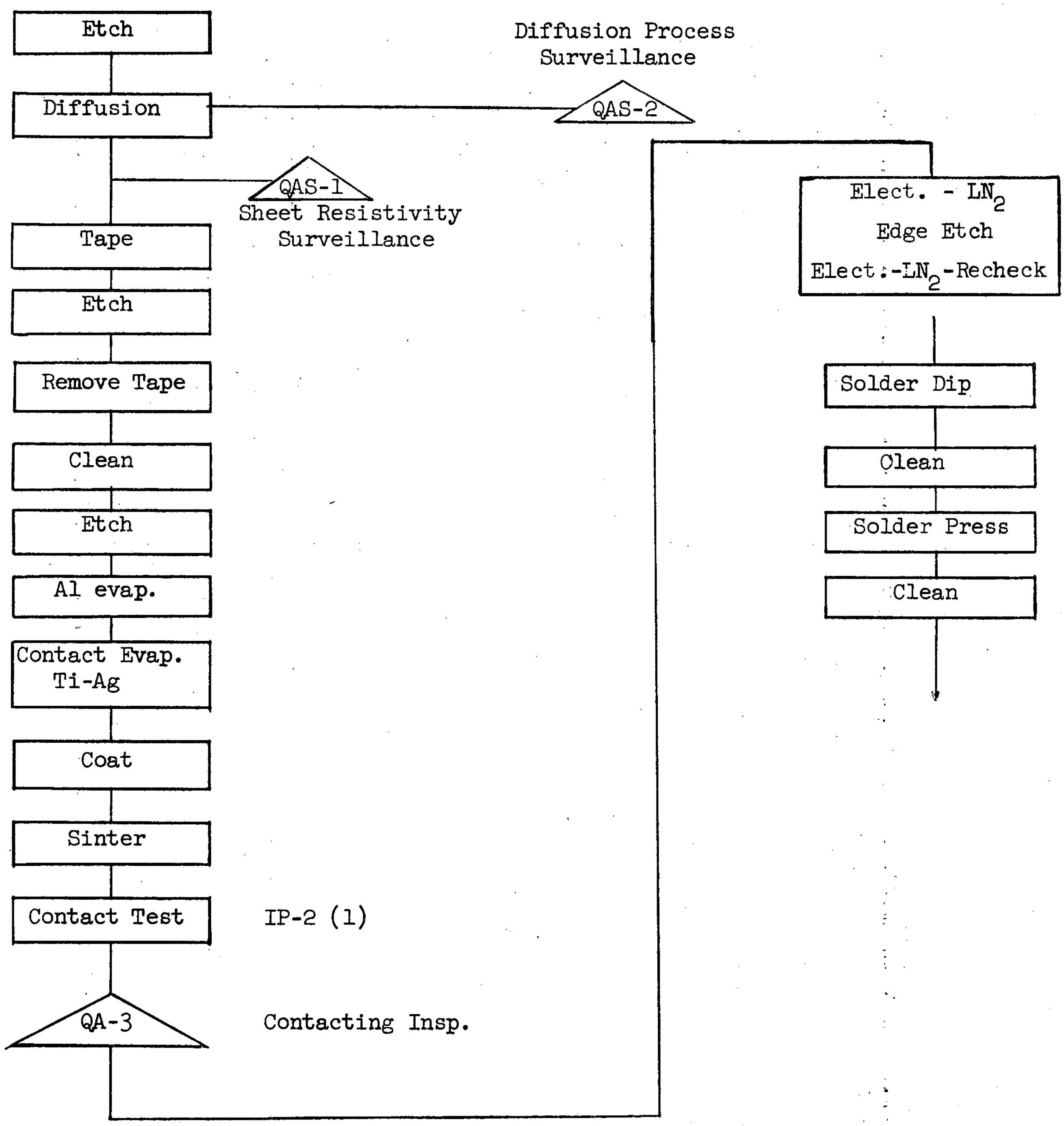

Fig. 22b

3.2 PILOT LINE RESULTS

3.2.1 Lot Variations

Rather than fabricate cells in all five lots exactly the same, Heliotek and NASA/Ames agreed that more information could be obtained if several minor cell variations were investigated: Table IV shows the differences between the five lots. The variations investigated included: contact configurations, silicon supplier, and back etch procedure; none had a significant effect upon cell output at low temperature and low intensity.

3.2.2 Electrical Characteristics

3.2.2.1 Dark Measurements at -196°C

As described in Section 2.6, measurement of the dark forward current at .9V, -196°C can be used to evaluate solar cell low temperature low intensity characteristics. This technique was utilized in the pilot production phase in order to 1) determine whether cells needed edge etching and 2) to enable us to correlate this dark measurement to the output of cells at 5.0 mw/cm^2 and -135°C. The solar cell I-V characteristic curve was measured from -1.0 to +1.0 volt to obtain information on the reverse as well as the forward characteristic. The forward current at .9V was divided into three categories:

1) 0-.2 mA (high output); 2) .2-.5 mA (borderline); 3) .5 mA+ (low output). The current distribution of all five lots before and after edge etching is shown in Table V. In all five lots, over half the cells exhibited currents at .9V well in excess of .5 mA, resulting, in most cases, from an extreme broken knee effect, but in some cases, from high leakage current due to metal over the junction edge. After edge etching, 50 to 85% of the cells had currents of .2 mA or less.

3.2.2.2 Measurements at 5.0 mw/cm^2, -135°C.

Cells were tested at 5.0 mw/cm^2 solar intensity and -135°C to determine output. Output can be determined by merely measuring the current at or near maximum power (in this case, .8V); however, I-V curves were

C.2

Table IV

Pilot Production Lot Characteristics

LOT#	SUBLOT	SUPPLIER	BACK ETCH	CONTACT CONFIGURATION
1.	38359A-1 -2	Texas Instruments	Std.	Bar Soldered
2.	36880A	Texas Instruments	Std.	Corner dart
3.	352-1 -1A	Monsanto	Std.	Corner Dart Bar Soldered
4.	352-2 -2	Monsanto	CP-4A	Bar
5.	38359	Texas Instruments	Std.	Narrow bar
	36880-1	Texas Instruments		Corner dart

Table V

Distribution of Dark Forward Currents of 10 ohm cm N/P

P+ Cells Fabricated in Pilot Production

Dark Forward current at .9V, measured at -196° before soldering

	Lot No.	Classification Before				Classification After Edge Treatment			
		A(1)	B(2)	C(3)	Total	A(1)	B(2)	C(3)	Total
1.	38359A-1	7	2	46	55	29	12	6	47
	-2	0	2	52	54	28	4	18	50
	-3	0	1	15	16	6	1	7	14
		7	5	115	125	63	17	31	111
2.	36880A	5	12	33	50	42	1	0	43
	B	5	13	38	56	46	4	6	56
	C	0	1	14	15	7	0	6	13
		10	26	85	121	95	5	12	112
3.	352-1	28	11	35	74	39	14	16	69
	352-1A	14	4	52	70	36	9	23	68
		42	15	87	144	75	23	39	137
4.	352-2A	4	1	44	49	32	9	6	47
	-2	9	0	54	63	40	11	12	63
		13	1	98	112	72	20	18	110
5.	38359	17	13	9	39	34	4	0	38
	36880-1	11	10	40	61	39	6	9	54
		28	23	40	100	73	10	9	92

(1) A I < .2 mA at .9V

(2) B .2 < I < .5 mA at .9V

(3) C I > .5 mA at .9V

recorded so that more information on the curve shape and I_{sc} could be obtained. The cells were classified into five output groups according to minimum current at .8V (as indicated in the Preliminary Specification):

I	3.0 mA
II	3.2 mA
III	3.4 mA
IV	3.6 mA
V	3.8 mA

Table VI shows the number of cells in each of these groups for all five lots. In all lots over half the electrically good cells (minimum current of 3.0 mA at .8V) were in Groups IV and V, corresponding to an efficiency of 14.4% or better. In the case of cells with corner darts, over half the cells had an efficiencies of 15.2% or better, due to higher I_{sc} and/or a greater degree of improvement in the curve factor with edge etching. Lot 2 cells exhibited the best efficiencies with 82% of the measured cells having efficiences ≥16.0% and 25% of the cells having efficiencies ≥16.8%.

The output distribution of cells in all five lots is shown in Figure 23. The output of 70% of the cells was 2.8 mW (3.5mA at .8V) or better, corresponding to an efficiency of 14% and above. Figure 24 shows the distribution of short circuit current measured at 5.0 mw/cm^2 solar intensity and -135°C. The medium short circuit current was 3.7 mA and the range was 3.7 to 4.4 mA.

Table VI

Output Distribution of Pilot Line Cells

Lot #	Sublot	Mech. Class.*	Group: Min. Current:	I 3.0	II 3.2	III 3.4	IV 3.6	V 3.8	Rejects <3.0
1	38359A-1,-2,-3	A		0	3	1	6	18	20
		B		6	2	5	2	2	
2.	36880-A,-~~B~~,C	A		0	3	1	3	56	4
	(corner dart)	B		0	0	0	0	10	
3.	352-1	A		0	1	3	6	22	7
	(corner dart)	B		0	0	2	3	12	
	352-1A	A		2	0	0	2	6	9
		B		1	0	2	0	0	
4.	352-2,-2A	A		2	3	9	20	27	17
		B		1	2	5	6	1	
5.	36880-1	A		1	0	3	15	15	10
	(corner dart)	B		0	2	2	5	4	
	38359	A		0	5	9	18	4	7
		B		3	0	1	5	0	

*Mechanical Classification

A - Cells have no defects such as chips, AR coating voids, etc.

B - Cells have defects; they meet specification requirements for output but not for physical characteristics.

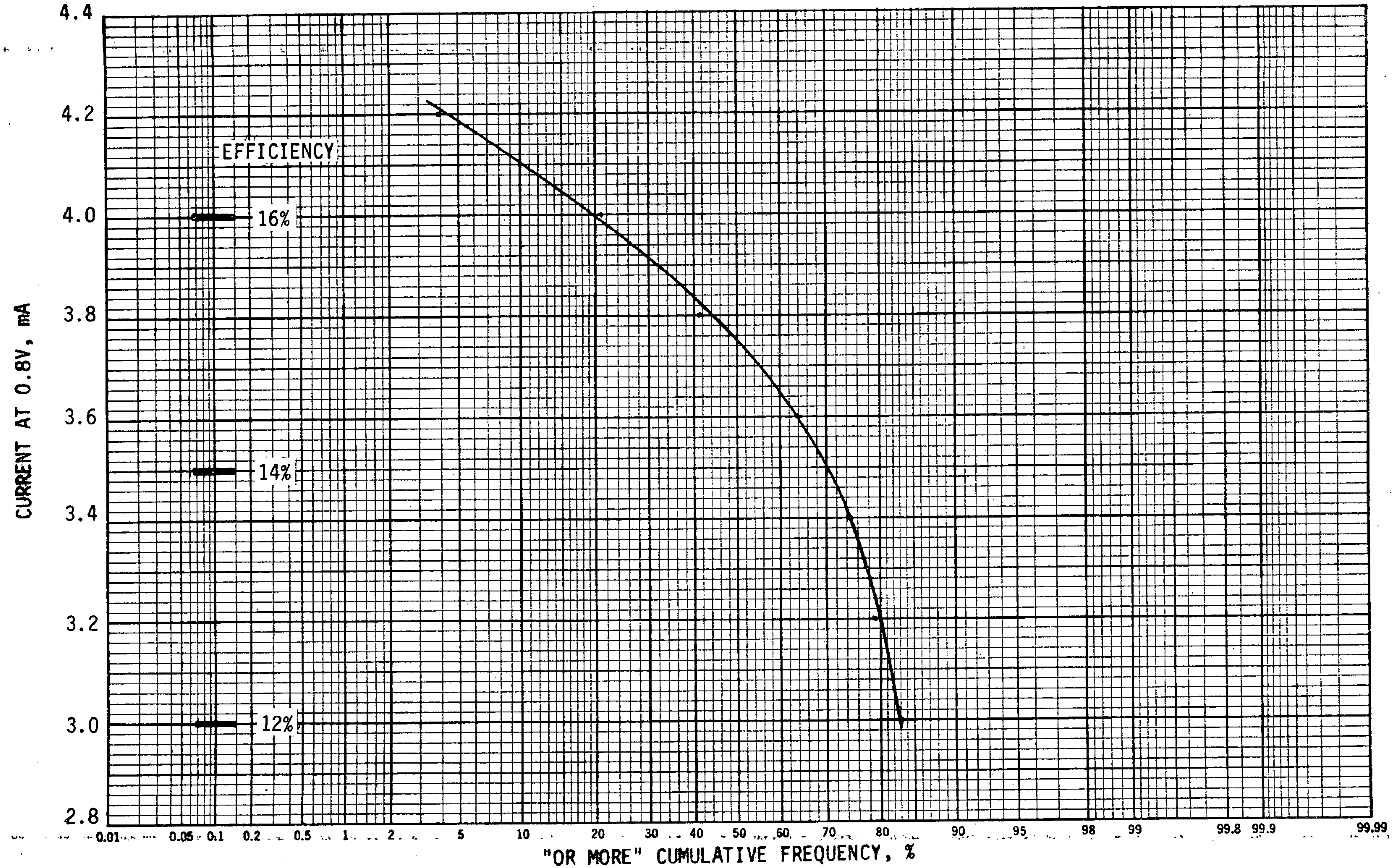

Figure 23. Output Distribution for Pilot Production Cells Fabricated for Low Temperature and Low Intensity Operation. Measured at 5.0 mW/cm^2 solar intensity and -135°C.

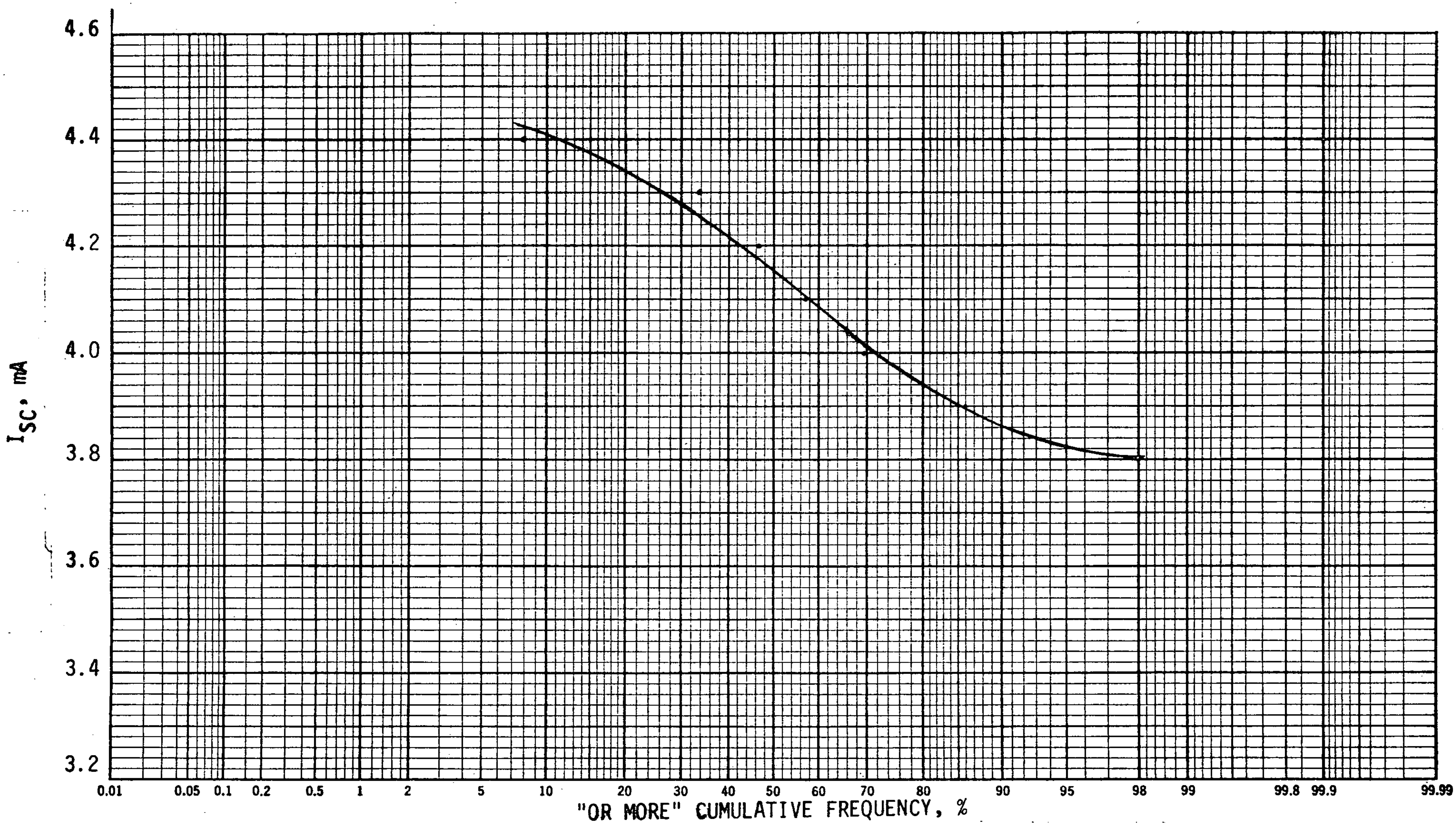

Figure 24. Short Circuit Current Distribution for Pilot Production Cells. Measured at 5.0 mW/cm^2 solar intensity and -135°C.

4.0 QUALIFICATION PROGRAM

In addition to the in-line QA inspection points and tests used to assure process control, once fabrication of cells was completed a qualification program was carried out. The purpose was to determine whether solar cells which had been fabricated using modified processes in order to improve the low temperature and low intensity performance, could still meet typical qualification and acceptance tests.

4.1 ACCEPTANCE TESTS

The test sequence is shown in Figure 25; the basic tests are a 45° pull test to evaluate contact strength and an AR coating adherence test. The AR coating test was performed by placing the cells in boiling water for 30 minutes, then abrading the surface with a grit free eraser for 20 strokes at 140 psi pressure, and observing whether any coating delamination occurred. None of the cells exhibited any coating delamination. For the 45° pull test only cells from lot 1, and part of lot 3 were included, since the rest of the cells were solderless and the tabs were supposed to be attached to the cells using no additional solder. I-V curves were measured before and after attaching tabs to evaluate any degradation; the measurements were performed at 5.0 mW/cm^2 and, for convenience, at 28°C rather than -135°C. Once tabbed and electrically tested, the cells were pull tested at a 45° angle to the cell surface. The electrical measurements showed no tabbing degradation and the pull strengths of these cells were in excess of the Preliminary Specification requirement of 500 grams (Table VII).

4.2 QUALIFICATION TESTS

The qualification test sequence (Figure 26) included 20 cycles from -140 to 85°C and a thirty-day exposure to 45°C, 90% relative humidity, with I-V curves measured before and after each test to determine

ACCEPTANCE TESTS AND TEST SEQUENCES

PLAN A

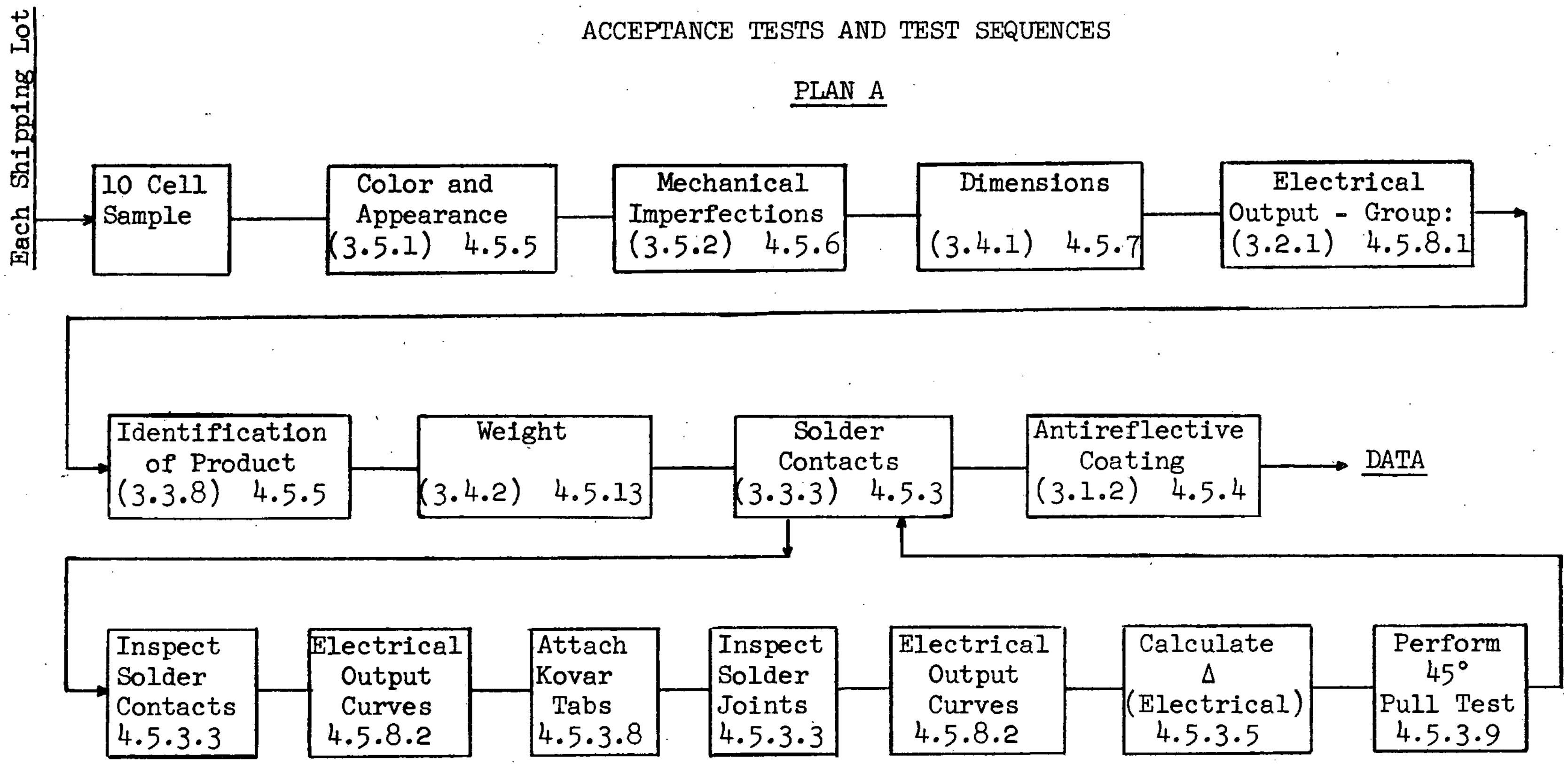

Fig. 25

TABLE VII

45° PULL TEST

Cell No.	I at .35 V, mA Before	After	* △	%	Pull Strength, Grams Front	Back
Lot 1						
1	3.94	3.99	+.05	1.25	900	1030
2	3.48	3.61	+.13	3.60	830	990
3	3.92	3.92	0	0	750	1050
4	4.05	4.01	-.04	0.99	1050	1020
5	4.08	4.03	-.05	1.22	1120	940
6	3.71	3.72	+.01	0.27	830	730
7	4.27	4.21	-.06	1.40	1080	720
8	4.10	4.10	0	0	1060	1050
9	4.01	3.99	-.02	0.50	1100	1050
10	3.99	3.99	0	0	800	850
Average	3.96	3.96	0	0		
Lot 3 a						
11	4.16	4.11	-.05	1.20	1100	1350
12	4.01	4.03	+.02	0.49	1000	900
13	4.13	4.12	-.01	0.24	970	1050
14	3.83	3.87	+.04	1.03	1000	1050
15	4.20	4.20	0	0	1050	790
Average	4.07	4.07	0	0		

* Measured at 5.0 mW/cm^2 and 28°C before and after attaching tabs to cell.

PLAN B

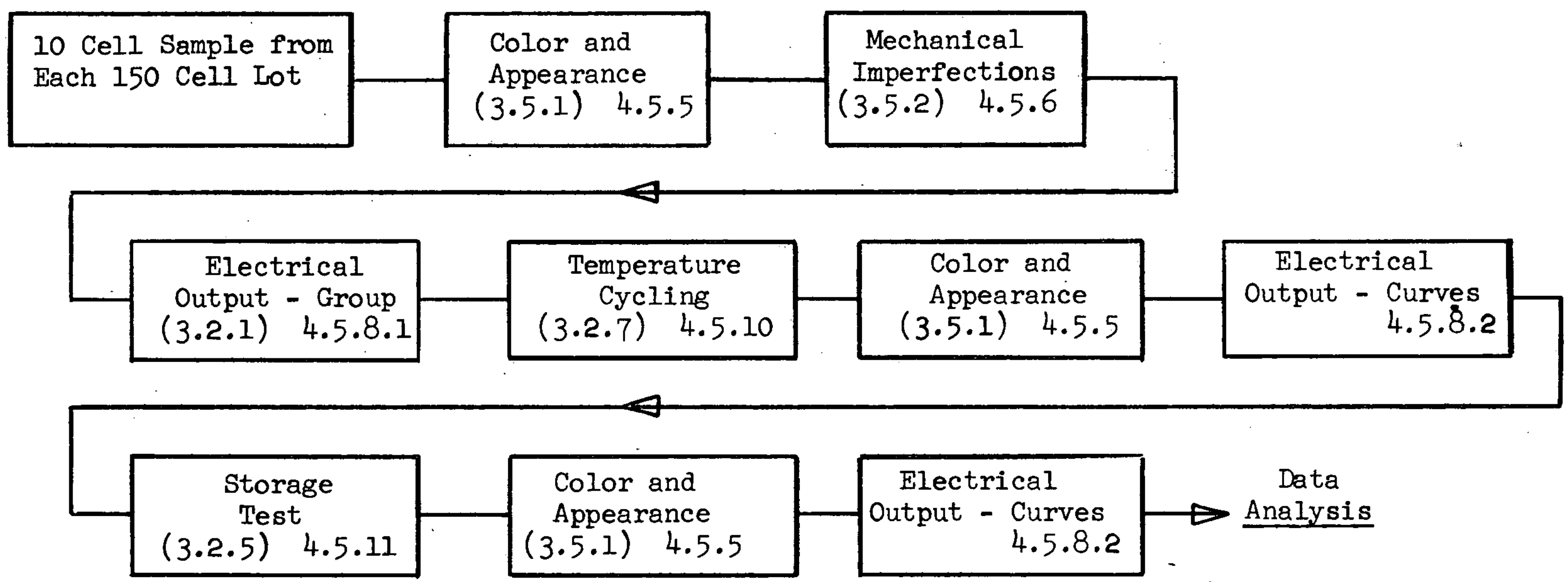

10 Cell Sample from Each 150 Cell Lot
Color and Appearance (3.5.1) 4.5.5
Mechanical Imperfections (3.5.2) 4.5.6
Electrical Output - Group (3.2.1) 4.5.8.1
Temperature Cycling (3.2.7) 4.5.10
Color and Appearance (3.5.1) 4.5.5
Electrical Output - Curves 4.5.8.2
Storage Test (3.2.5) 4.5.11
Color and Appearance (3.5.1) 4.5.5
Electrical Output - Curves 4.5.8.2
Data Analysis

Fig. 26

degradation. Ten cells from each lot were subjected to temperature cycling; the resulting average degradation was less than 1% for all five lots. (Table VIII)

Only soldered samples from lots 1 and 3 were subjected to the humidity test. The average current degradation for samples in both lots was zero.

TABLE VIII

ELECTRICAL CHARACTERISTICS * BEFORE AND AFTER TEMPERATURE CYCLING

Cell No.	I at .35 V, mA				Cell No.	I at .35 V, mA			
	Before	After	△	%		Before	After	△	%
Lot I					Lot 4				
1	4.12	4.12	0	0	31	4.31	4.33	+.02	+0.46
2	4.21	4.17	-.04	-0.95	32	3.86	3.90	+.04	+1.03
3	4.08	4.06	-.02	-0.49	33	4.10	4.11	+.01	+0.24
4	4.29	4.22	-.07	-1.63	34	4.14	4.12	-.02	-0.48
5	4.17	4.16	-.01	-0.24	35	4.18	4.18	0	0
6	3.05	3.20	+.15	+4.69	36	4.13	4.14	+.01	+0.24
7	3.82	3.81	-.01	-0.26	37	4.31	4.33	+.02	+0.46
8	3.94	3.98	+.04	+1.00	38	4.35	4.32	-.03	-0.69
9	4.09	4.10	+.01	0	39	4.38	4.35	-.03	-0.68
10	4.17	4.17	0	0	40	4.27	4.25	-.02	-0.47
Average	3.99	4.00	+.01	+0.25	Average	4.20	4.20	0	0
Lot 2					Lot 5				
11	4.30	4.38	+.08	+1.18	41	3.93	4.00	+.07	+1.75
12	4.35	4.30	-.05	-1.15	42	4.14	4.17	+.03	+0.72
13	4.48	4.41	-.07	-1.56	43	4.02	4.03	+.01	+0.30
14	4.31	4.30	-.01	-0.23	44	3.82	3.82	0	0
15	4.39	4.35	-.04	-0.91	45	4.07	4.07	0	0
16	4.45	4.42	-.03	-0.67	46	4.05	4.01	-.04	-0.99
17	4.49	4.47	-.02	-0.45	47	4.02	4.00	-.02	-0.50
18	4.34	4.30	-.04	-0.92	48	4.08	4.02	-.06	-1.47
19	4.50	4.47	-.03	-0.67	49	3.92	3.90	-.02	-0.51
20	4.50	4.50	0	0	50	4.08	4.02	-.06	-1.47
Average	4.41	4.39	-.02	-0.45	Average	4.01	4.00	-.01	-0.25
Lot 3									
21	4.47	4.50	+.03	+0.67					
22	4.29	4.25	-.04	-0.93					
23	4.53	4.53	0	0					
24	4.19	4.44	+.25	+5.64					
25	4.39	4.37	-.02	-0.45					
26	3.35	3.40	+.05	+1.05					
27	3.87	3.87	0	0					
28	4.06	4.00	-.06	-1.48					
29	4.18	4.16	-.02	-0.48					
30	4.16	4.17	+.01	+0.24					
Average	4.15	4.17	+.02	+0.48					

* Measured at 5.0 mW/cm^2, 28° C.

5.0 CONCLUSIONS

High resistance or rectifying characteristics typically observed at low temperature with TiAg contacts due to metal-semiconductor barrier formation are effectively eliminated by alloying Al into the back surface of an N/P solar cell to form a P+ region. A low temperature ohmic contact increases the solar cell maximum power voltage at 5.0 mW/cm^2 and -135°C from .7 V to .8 V, corresponding to an output improvement of $\sim$ 15%.

Both low shunt resistance and the broken knee effect reduce cell current and voltage at maximum power; the reduction in power can vary from a few per cent to more than 50%. Shunt resistance can be increased by diffusing a deeper junction and etching the cell edges to remove metal or other contaminants which produce current leakage paths. The same etch procedure used to remove current leakage paths which cause low shunt resistance can be used to minimize or eliminate the "broken knee" effect.

The wide range in short circuit current at -135°C observed with crucible grown silicon due to variations in $\Delta I_{sc}/\Delta T$ can be reduced considerably by using low oxygen, low dislocation density silicon, such as Mon-X or Lopex. Use of Mon-X or Lopex silicon minimizes the short circuit current change, such that the lowest currents measured at 5.0 mW/cm^2 and -135°C for pilot production cells was 3.7 mA, whereas with crucible grown silicon short circuit currents as low as 2.0 mA have been measured.

The improvement in cell output at low temperature and low intensity using the techniques discussed above was demonstrated in the pilot production phase. Seventy percent of the cells had efficiencies of 13 to 17%. The pilot production phase also demonstrated the feasibility of using the modified procedures on a production basis.

This type of cell as well as exhibiting improved electrical performance meets typical requirements for space quality cells. This was demonstrated by subjecting samples to humidity, temperature cycling, coating adherence, and contact strength tests.

6.0 RECOMMENDATIONS

Additional refinement in the edge etching technique used to eliminate current leakage paths is needed since the improvement in curve shape and output obtained with this technique varies. The low output cells in the pilot production phase were those which showed less improvement with edge etching. Changes in this process which could improve the uniformity of the results include: 1) A substitute for tape masking since the etch will vary according to the amount of tape trimmed from the edges and the presence of adhesive on the cell edges, or 2) use of a mesa etch.

Since the coefficient of expansion of silicon and solder is quite different, the stress at extremes of temperature can be severe enough to shear silicon. This would also be a problem if soldered interconnect joints were made. A solderless cell is recommended based on the characteristics of the solder-silicon system and the temperatures encountered. There are currently two solderless contact systems which exhibit humidity resistance comparable to the soldered TiAg contact, 1) TiPdAg and 2) Al. In this case, Al would be an attractive choice since it can be used to form both the P+ region and the contact.

At low intensity, the effect of series resistance becomes less significant; therefore, the contact area and number of grid lines can be reduced to obtain more active area. The active area could be increased 5%, using a wraparound contact and reducing the number of grid lines, without encountering the typical problems of wraparound contacted solar cells at high intensity. At high intensity, as the P contact is reduced series resistance increases. It is necessary, therefore, to minimize the N wraparound region and the spacing between the N region and the P contact. This makes it difficult to evaporate the contact without getting metal across the junction and high leakage currents are typically a problem unless very tight mask tolerances are used in the etching and contacting operations. With the reduction in the effect of series resistance at low intensity, the N region could be increased with the N contact area kept the same, e.g., the typical N region width of

$\sim .050''$ could be increased to $.100''$ with the N contact width of $.040''$ kept the same. This would reduce the possibility of evaporating the N contact across the junction. Increasing the spacing between the N region and the P contact would also reduce the possibility of evaporating metal across the junction. Theoretically and practically the wraparound contact should be ideal for low intensity application and should be investigated.

REFERENCES

(1) C. H. Liebert, "Solar Cell Performance at Jupiter Temperature and Solar Intensity," Presented at Seventh IEEE Photovoltaic Specialists Conference, Pasadena, Calif., Nov. 19-21, 1968.

(2) C. H. Liebert and R. E. Hart, Jr., "Solar-Cell Performance at Low Temperatures and Simulated Solar Intensities," NASA TN D-5547, 1969.

(3) R. J. Lambert, "Characteristics of Solar Cells at Low Temperatures," Conference Record of the Seventh Photovoltaic Specialists Conference, IEEE, pp. 97-100; 1968.

(4) E. L. Ralph, "Performance of Very Thin Silicon Solar Cells," Conference Record of the Sixth Photovoltaic Specialists Conference, Vol. 1, IEEE, pp. 98-116; 1967.

(5) W. Crawford Dunlap, Jr., An Introduction to Semiconductors, John Wiley & Sons, Inc., New York 1957, p. 193.

(6) Aldert van der Ziel, Solid State Physical Electronics, Prentice-Hall, Inc., New Jersey, 1968, pp. 101, 269.

(7) A. J. Goss and R. E. Adlington, Solid State Physics in Electronics and Telecommunications, Vol. 1 (ed. M. Desirant and J. L. Michiels), Academic Press, London and New York (1960), pp. 28-42.